ACCIMA: A Regional Climate System Model for the Southern Ocean and Antarctica*

David H. Bromwich[1,2], Changhyun Yoo[3], Keith M. Hines[1**], Lesheng Bai[1]

John M. Klinck[4], David M. Holland[3], Michael S. Dinniman[4], and Edwin P. Gerber[3]

[1]Polar Meteorology Group, Byrd Polar Research Center

The Ohio State University, Columbus, Ohio

[2]Atmospheric Sciences Program, Department of Geography

The Ohio State University, Columbus, Ohio

[3]Center for Atmosphere Ocean Science, Courant Institute of Mathematical Sciences

New York University, New York, New York

[4]Department of Ocean, Earth and Atmospheric Sciences

Center for Coastal Physical Oceanography, Old Dominion University, Norfolk, Virginia

Submitted to *Journal of Climate*

[**]Corresponding Author Address: Keith M. Hines

Polar Meteorology Group, Byrd Polar Research Center

The Ohio State University, 1090 Carmack Road

Columbus, OH 43210-1002, email: hines.91@osu.edu

[*]Contribution XXXX of the Byrd Polar Research Center

Abstract

The Atmosphere-Ocean Coupling Causing Ice Shelf Melt in Antarctica (ACCIMA) project has adapted a regional coupled atmosphere, ocean, sea-ice and land model to the polar Southern Hemisphere with sufficient spatial resolution to capture key physical processes in each component model. The motivation is to understand the mass balance of the Antarctic Ice Sheet-a critical element of projections of global sea-level change. Mesoscale processes in the ocean, atmosphere, and on land contribute. The project seeks to better understand ice shelf retreat in the Amundsen Sea embayment of West Antarctica, that is contributing significantly to sea-level rise, by analyzing processes in the atmosphere and ocean that influence the delivery of heat to the floating ice shelves which causes them to melt. The coupled model for ACCIMA, similar to that used in the Regional Arctic System Model project, is a limited-area model based upon the Community Earth System Model (CESM) framework with the CESM flux coupler linking model components. These models include the polar optimized version of the Weather Research and Forecasting Model, the Los Alamos sea-ice model, the Parallel Ocean Program, and the Community Land Model. Coupled simulations have been run for 1999-2010 driven by the ERA-Interim global atmospheric reanalysis and climatological conditions around the ocean boundary. Realistic wind patterns develop over the continent and near the Antarctic coast in response to land topography. SST compares well to observations but is a bit warm in the south and cold in the north. Sea-ice extent is realistic but is low in summer. Coastal ocean heat content declines over the simulation.

1. Introduction

Understanding the mass balance of the Antarctic ice sheet is critical for projecting global sea-level change (Rignot et al. 2011). During the past few decades, mass loss from the ice sheet has accelerated (Chen et al. 2009; Velicogna 2009; Rignot et al. 2011) with the most significant changes being in the thickness of the grounded portions of the ice sheet observed at the coastal margins (Pritchard et al. 2009). The climate issues revolving around the ice mass balance represent the primary motivation for the Atmosphere-Ocean Coupling Causing Ice Shelf Melt in Antarctica (ACCIMA) project. On decadal and shorter timescales, the Antarctic Ice Sheet is linked to climate phenomena with global signatures including the El Niño-Southern Oscillation, the Southern Annular Mode, Atlantic Multidecadal Oscillation, and the Interdecadal Pacific Oscillation (e.g., Turner 2004, 2007; Fogt et al. 2011; Okumura et al. 2012; Steig et al. 2013; Li et al. 2014). The processes that impact the Antarctic Ice Sheet span both a range of physical domains (the atmosphere, ocean and ice), and a range of spatial scales. In particular, mesoscale processes in the atmosphere and ocean deliver heat to the bottom of the floating ice shelves, especially in the Amundsen Sea embayment (Jacobs et al. 2012). Accordingly, our coupled modeling project endeavors to encompass all the system processes that *melt Antarctic ice shelves* at the sufficient resolution to capture the mesoscale of the atmosphere and ocean.

The West Antarctic Ice Sheet (WAIS, Fig. 1), although much smaller than the East Antarctic Ice Sheet, is particularly important for sea level change as it is much more sensitive to climate change (Steig et al. 2009; Okumura et al. 2012; Bromwich et al. 2013a; WAIS Divide Project Members 2013). The WAIS loses volume due to outlet glaciers draining into the Amundsen Sea (Thomas et al. 2004; Pritchard et al. 2009). The floating portions of the ice sheet, known as ice shelves, are thought to buttress the outlet glaciers (DeAngelis and Skvarca 2003; Dupont and

Alley 2005; Schoof 2007). Ice shelf mass changes result in changes in the flow of continental ice off the land thus altering sea level. Until recently, iceberg calving was thought the most significant mass loss from the floating ice shelves, but new studies suggest slightly more mass is lost from basal melting (Depoorter et al. 2013; Rignot et al. 2013). One proposed reason for the supposed increased basal melt of ice shelves in the region is a change in either the temperature or circulation of warm Circumpolar Deep Water (CDW) that enters the subglacial volume providing heat to increase the basal melt rate (Payne et al. 2004).

Along some parts of the Amundsen and Bellingshausen Sea sectors (roughly, 80-130°W, Fig. 1), the edge of the WAIS is within 100 km of the continental shelf break, although along others, it can be more than 300 km away. Orsi et al. (1995) define the southern terminus of upper CDW as the poleward boundary of the Antarctic Circumpolar Current (ACC, see Fig. 1), and in the Bellingshausen Sea this abuts the continental shelf break and contains water with temperatures up to 1.8°C. In the Amundsen-Bellingshausen sectors of the South Pacific Ocean, CDW is observed to intrude onto the continental shelf, and advection of this warm water across the continental shelf to the base of ice shelves is thought to supply the majority of the heat involved in the basal melt of several of the shelves along the coast in the Amundsen (specifically Pine Island Glacier: Jacobs et al. 1996; Jenkins et al. 1997; Hellmer et al. 1998; Walker et al. 2007) and Bellingshausen Seas (Potter and Paren 1985; Talbot 1988; Jenkins and Jacobs 2008). This fact gives rise to the hypothesis that changes in the intrusions of this warm oceanic water under the ice shelves are an important cause for the recently observed increase in ice thinning. It should be noted, however, that other recent studies suggest the melting in the Bellingshausen ice shelves is more driven by variability of the upper-ocean conditions than by flux of CDW across the continental shelf (Holland et al. 2010; Padman et al. 2012). Representing all these processes in a coupled model system presents a major challenge.

Ice shelf basal melting occurs by three modes (Jacobs et al. 1992) with one or more modes active at any time. Mode-1 involves High Salinity Shelf Water (HSSW), a cold, salty water mass formed near the ice shelf during winter that subducts into the sub ice-shelf cavity causing modest melting by depressing the melting point with over-burden pressure. Rapid mode-2 melting is induced by the flooding of warm, salty CDW into the cavity. Mode-3 melting occurs near the ice shelf front, driven by summertime warming of Polar Surface Waters that subduct beneath the ice front, partly driven by tidal and regional circulation forcing. Given the importance of basal melt, in all its modes, to ice sheet evolution, and thus to sea-level change, an overarching goal of this project is to understand recent apparent mode-shifts in basal melt of ice shelves in Antarctica, and to project possible future changes.

Both regional and small horizontal scale atmospheric forcing can be relevant to ocean transport of heat to the ice shelves. Model studies in the Amundsen (Thoma et al. 2008) and Bellingshausen (Dinniman et al. 2011) suggest that the winds along the shelf-break force intrusions of CDW across the continental shelf. Recent comparisons of measured currents to winds in the Amundsen Sea (Carvajal et al. 2013; Wåhlin et al. 2013) appear to confirm this. Finer scale winds increase the fidelity of simulations of coastal polynyas in the Weddell (Hollands et al. 2013) and Ross Seas (Petrelli et al. 2008; Mathiot et al. 2012) compared to coarse resolution wind simulations. Fine winds also improve the simulated properties of the Ross Sea HSSW (Mathiot et al. 2012). Better simulation of coastal sea ice would more accurately represent the creation of HSSW (mode-1 melting), improve the vertical mixing of heat from CDW (mode-2 melting, e.g. Holland et al. 2010), and improve surface heating in ice-free areas (mode-3 melting). An ocean/sea ice/ice shelf simulation (Dinniman et al. 2014) shows a 15% increase in the total Antarctic ice shelf melt when finer scale winds are used.

Not only are regional-scale atmospheric changes important drivers of changes in the ocean, but small horizontal scale atmospheric forcings can be crucial for oceanic processes that are relevant to ocean transport of heat to the ice shelves. For example, the observed frequency of intrusions of CDW from the abyssal ocean onto the continental shelf (Moffat et al. 2009) suggests that the winds along the shelf-break are critical in forcing the intrusions, and recent model studies in the Amundsen (Thoma et al. 2008) and Bellingshausen (Dinniman et al. 2011) highlight the importance of the winds. In the Ross Sea, the Terra Nova Bay polynya, which is forced by persistent westerly katabatic winds flowing off the Victoria Land Coast (Bromwich et al. 1993) , is crucial to the creation of HSSW on the continental shelf and has an effect on the transport of water masses (and heat) underneath the Ross Ice Shelf.

In this paper, we introduce the primary tool for ACCIMA, a high-resolution coupled regional ice-ocean-atmosphere-land model. As detailed in Section 2, the model is capable of receiving boundary data from global sources and downscaling that forcing to the fine spatial scales appropriate for a regional model. In Section 3, a simulation over the 12-year period from 1999 to 2010 is assessed to validate the fidelity of the model, with particular focus on the mesoscale processes in the ocean, atmosphere and sea-ice that contribute to the basal melting of ice shelves, including the southward transport of heat and the northward transport of freshwater. Relatively coarse resolution coupled ocean-atmosphere simulations forecast, or at least suggest, increased ice shelf melting (e.g., Overpeck et al. 2006), and current observations indicate a reduction in ice volume and increased transport of ice sheets towards the ocean (Pritchard et al. 2009). We frame the ACCIMA project in this larger context, and sketch out future research objectives, in Section 5.

2. The ACCIMA Modeling System

The modeling system for ACCIMA includes four widely-used component models linked through the National Center for Atmospheric Research (NCAR) Community Earth System Model (CESM, Hurrell et al. 2013) flux coupler CPL7 (Craig et al. 2012). The regional system for high southern latitudes originates from a version of the Regional Arctic System Model (RASM, Cassano et al. 2011; Maslowski et al. 2012; http://www.oc.nps.edu/NAME/RASM.htm) that we obtained from Tony Craig of NCAR. RASM and ACCIMA have the basic modular framework of the CESM. The ocean model (POP2) and the sea ice model (CICE) are part of the ACCIMA system. While RASM uses the Variable Infiltration Capacity (VIC, Liang et al. 1994) for the land model, ACCIMA uses the Community Land Model (CLM), which is the original CESM land model and can represent ice-covered high latitude land. Finally, ACCIMA, similar to RASM, uses the Weather Research and Forecasting model (WRF, Skamarock et al. 2008) for the atmosphere in place of the Community Atmosphere Model (CAM) used in CESM. These component models are discussed in more detail below.

a. Polar WRF

For the atmosphere we use WRF version 3.2 with inclusion of polar-optimizations, such as fractional sea ice (Hines and Bromwich 2008; Bromwich et al. 2009). The land surface models inside WRF are not active because of the coupling to CLM. The polar-optimized version of WRF (Polar WRF) has been tested in the Arctic for the Greenland Ice Sheet (Hines and Bromwich 2008), the Antarctic region (Powers et al. 2012; Bromwich et al. 2013b), the Arctic Ocean

(Bromwich et al. 2009) and Arctic Land (Hines et al. 2011; Wilson et al. 2011, 2012). For Antarctica, Polar WRF is now the only model for operational forecasting in support of National Science Foundation's operations including transportation and field programs (Powers et al. 2012).

Extensive experimentation was done with the standalone Polar WRF on the ACCIMA grid with 30 km grid spacing to find the optimal setup for these simulations. WRF physical parameterizations selected for use in the coupled-model simulations include the MYNN2 2.5-level boundary layer scheme (Nakanishi and Niino 2006) with the Monin-Obukhov surface boundary layer. For radiation, both the CAM longwave and shortwave schemes are used. Cloud microphysics are treated by the Goddard scheme (Tao et al. 1989), while cumulus convection is parameterized through the Kain-Fritsch scheme (Kain 2004). WRF simulations use 39 vertical layers with lowest layer centered near 12 m above ground level, and the model top is at 50 hPa. Over the ocean, 10 layers are within 1000 m of sea level.

b. POP2

The Parallel Ocean Program (POP2, Smith et al. 2010; Danabasoglu et al. 2012) represents the ocean. POP2 is a public model with depth as vertical coordinate designed for generalized orthogonal grids and derived from earlier ocean models (e.g., Bryan 1989). Ocean geometry and bathymetry are represented by stacked boxes with heights of 10 m near the surface and increasing to 250 m at the bottom. The deepest parts of the ocean are represented by 50 boxes. Slower baroclinic modes are integrated explicitly, while the fast barotropic modes are integrated implicitly with a free surface methodology. Horizontal viscosity and diffusivity is based on the biharmonic operator with coefficients of -27×10^9 m^4s^{-1} for momentum and -3×10^9 m^4s^{-1} for tracers. Vertical mixing uses the K-profile parameterization with background diffusivity ranging from 10^{-5} m^2s^{-1} near the surface to 10^{-4} m^2s^{-1} at depth. Large diffusivity and viscosity (0.1 m^2s^{-1}) are used to simulate convection. Dense water is created in the coastal areas around Antarctica. Special formulations are included to transport dense water to depth without excess mixing (Briegleb et al. 2010).

Surface fluxes of momentum, heat and freshwater are provided by the coupler. The outer boundary of the model domain are solid walls (open boundary conditions are not specified in this version of POP2). The ocean is nudged to monthly averaged temperature and salinity obtained from ECCO2 (Estimating the Circulation and Climate of the Ocean, Phase II; Wunsch and Heimbach 2007) in a boundary zone equatorward of 50°S. The restoring time scale is three months at the model boundary tapering to infinity at 50°S.

c. CICE

The comprehensive Los Alamos Community Ice CodE (CICE version 4.1, Hunke and Lipscomb 2008) represents sea ice. It includes thermodynamics, dynamics and horizontal transport of sea ice over a grid of points. The ice model uses four layers of ice and one layer of snow in each of five ice thickness categories (and one category for open water) to represent different types and ages of sea ice. The thermodynamic model (Bitz and Lipscomb 1999) calculates the local growth rate of snow cover and sea ice. The elastic-viscous-plastic rheology model (Hunke and Dukowicz 1997) is used to calculate internal ice stress. Ice advection is represented by the incremental remapping scheme (Lipscomb and Hunke 2004).

Stress boundary conditions are imposed at the upper boundary (wind stress) and lower boundary (ocean drag) with atmosphere and ocean conditions coming from the coupler. The new melt pond and surface albedo formulations (Holland et al. 2012) are included.

d. CLM4

The Community Land Model version 4 (CLM4, Oleson et al. 2010; Lawrence et al. 2011) which includes the SNow and ICe Aerosol Radiation (SNICAR) model for the snowpack (Flanner et al. 2007) represents land processes. CLM4 has updated snow cover parameterizations and accounts for snow aging based upon snow grain size. Solar snow albedo is computed over five spectral bands. CLM4 has slightly brighter albedos over Antarctica and snow aging is slower than in earlier versions. Up to five snow layers are treated by CLM4. Beneath the snow layers, 15 subsurface levels extend from a depth of 0.071 m at the top to 35.18 m at the bottom.

e. Grid configuration

The ACCIMA grid for the coupled simulations was selected after testing with individual component models. The grid shown in Fig. 1 is designed to demonstrate the performance of coupled simulations for modern climate. Higher-resolution simulations will be performed to detail the multi-disciplinary physics of Antarctic ice shelf melting. The current ACCIMA grid covers a square 10,560 km by 10,560 km polar stereographic domain centered over the South Pole. The domain captures most of the Southern Ocean (taken to be the ocean south of the southern Subtropical Front) including the key circumpolar oceanic fronts (Fig. 1). A fine (10 km spacing) basic grid was developed; coarser grids, including that currently used, are obtained by subsampling this basic grid. The simulations described here employ a grid with 60 km spacing for the atmosphere, which is the most cpu-intensive component of the coupled system. The land model has the same resolution, while finer resolution (20 km spacing) is used for the ocean and sea ice models to capture increased eddy activity in the Southern Ocean

f. *Forcing*

The Polar WRF atmosphere in this regional coupled simulation is driven at the lateral boundaries by the ERA-Interim Reanalysis (ERA-I, Dee et al. 2011) from the European Centre from Medium-Range Weather Forecasts (ECMWF). Evaluations of global reanalyses show that ERA-I well represents conditions in the polar Southern Hemisphere compared to other reanalyses (Bromwich et al. 2011).

The southern polar domain presents a particular challenge for regional atmospheric modeling because the outer boundary is roughly parallel to the mean flow; specified conditions around the boundary provide insufficient information about weather systems in the domain. In addition, much of the interior of our domain is too far from the boundaries (more than the deformation radius) to be sufficiently constrained. We therefore combine specified lateral boundary conditions (all atmospheric variables are updated from the global reanalysis every 3 hours) with atmospheric spectral nudging throughout the interior of the domain (e.g., Glisan et al. 2013). Nudging is applied to spatial scales larger than wavenumber 7 (> 1500 km) for horizontal wind, temperature, and geopotential height above 300 hPa to ensure that the large-scale structure of the circulation is consistent with ERA-I; however, the atmospheric mesoscale circulation is allowed to evolve freely.

g. *Initialization*

The ocean, sea ice, and land models have relatively long adjustment scales so these models were integrated separately to allow them to adjust to initial conditions. The ocean/sea ice and land models are first integrated (uncoupled) from climatological initial conditions (e.g., ECCO2 for the ocean and Qian et al. 2006 for land) to an equilibrium state forced by the prescribed atmosphere using version 2 Common Ocean-ice Reference Experiments dataset (Large and Yeager 2008). All models were then integrated with coupling for three additional years with the Polar WRF atmosphere forced by repeating ERA-I conditions for 1999 to allow the models to adjust.

3. Results

The coupled model with the 60 km atmosphere and land and the 20 km ocean and sea ice grids was integrated from 1999 to 2010. The NCAR Yellowstone computing system required approximately 3 days of wall-clock time (using 528 processors) to complete one year of simulation. The solutions of the various component models are compared to measured quantities to evaluate the realism of these calculations.

a. Atmosphere

The diagnostics for the atmosphere model are the pressure reduced to sea level, the wind velocity at 10 m height above ground, air temperature at 2 m height, precipitation, surface energy fluxes and the surface radiation balance. These are the most relevant quantities for coupling to the ocean, ice and land. We compare these fields to those of ERA-I. The global reanalysis will be very close to observations for fields referred to as “Class A” by Kalnay et al. (1996) that are strongly constrained, such as surface pressure. For “Class C” fields such as precipitation and sensible heat flux, reanalysis values are not directly constrained and will depend upon the model used for the assimilation. This limits quantitative evaluations. Nevertheless, ERA-I provides realistic Class C fields for comparison.

The simulated multi-year (1999-2010) average sea level pressure (Fig. 2a) displays characteristics of ERA-I (Fig. 2b) in the Southern Hemisphere, including the strong zonally-symmetric pattern north of 60°S, the circumpolar trough between 60-70°S, and higher pressure in the subtropics. The pressure in the trough has a wave number three pattern with the lowest pressure 979 hPa over the Ross Sea. This deep low migrates westward to the Amundsen Sea during summer (not shown). The low over the Indian Ocean near 90°E is about 1 hPa too deep and perhaps 10° east of its position in the reanalysis. Because the Antarctic Plateau is at high altitude, sea level pressure (a derived quantity) may not reflect the true horizontal surface pressure gradient over the continent, and thus is not shown.

The average 10-m wind velocity (Fig. 3a) has the expected strong westerlies over 40-60°S which provide the driving force for the ACC. Over Antarctica, the katabatic surface winds are downslope and turned to the left by the Coriolis force. The winter (June-July-August) mean (1999-2010) katabatic winds (Fig. 3b) not only clearly show the downslope drainage pattern but also show how these winds extend offshore over the ocean. Over the Ross Ice Shelf, stronger winds occur toward the southern and western edges. The winter average 2-m temperature over the high East Antarctic Plateau (Fig. 3b) show very cold air as the source of these flows. Wind speeds of 10-15 m s^{-1} are seen along the escarpment of East Antarctica and near the Transantarctic Mountains. Over the Antarctic continent the annual-average near-surface atmospheric temperature agrees well with climatological fields (e.g., Briegleb and Bromwich 1998a). A strong gradient occurs over the coastal escarpment, especially over East Antarctica. There the temperature difference between the upper and lower sections of the escarpment can exceed that associated with the adiabatic lapse rate.

Annual-average precipitation for 1999-2010 (Fig. 4) is a stricter diagnostic for the atmospheric model, and it compares well to that from ERA-I. Spectral nudging maintains the larger scale structure of the atmosphere, but does not directly constrain the atmospheric water content that contributes to precipitation. The area shown in Fig. 4 is reduced from the model domain as precipitation near the boundaries is impacted by the specified boundary condition of zero precipitation at the edge of the WRF domain. Less than 10 cm of water-equivalent precipitation falls over interior East Antarctica, while interior West Antarctica receives more precipitation with typical values of 10-20 cm. A narrow maximum is also found on the western side of the Antarctic Peninsula (Fig. 4b). Over 400 cm falls near the windward side of southern South America. ACCIMA produces more precipitation than ERA-I over the Pacific Ocean for 50-60°S and over the Antarctic coastal waters of the Indian Ocean.

Realistic precipitation is critical for maintaining ocean stratification and providing freshwater to coastal ocean in areas such as the west side of the Antarctic Peninsula. Precipitation minus evaporation (P-E) is a key input to the ocean, and ERA-I produces estimates of precipitation for the Southern Ocean near the average of modern reanalyses and less than the Global Precipitation Climatology Project (Bromwich et al. 2011). The zonal mean difference between ACCIMA and ERA-I for precipitation, evaporation, and P-E over interior Antarctic latitudes are small (Fig. 5). ACCIMA simulates 4-6 cm yr^{-1} more precipitation and P-E, while the evaporation/sublimation difference is very small. Over the Southern Ocean latitudes, ACCIMA simulates more precipitation than ERA-I by up to 15 cm yr^{-1} which is balanced, however, by increased evaporation in ACCIMA so that P-E is just 4-7 cm yr^{-1} larger for 65-75°S. North of 60°S, the evaporation difference exceeds that of precipitation, and P-E is less in ACCIMA than that of ERA-I. Generally, the differences are small so precipitation results are encouraging for the coupled model. In summary, ACCIMA captures the basic pattern of an arid Antarctica with precipitation generally increasing to the north over the ocean. The model is able to reproduce the large-scale precipitation structure based only on the moisture content at the lateral boundaries.

The surface shortwave radiation is important for surface heating over land and the ocean and is strongly influenced by the atmospheric model's cloud processes. Furthermore, over 90% of the incident shortwave radiation will be absorbed in the mid-latitude ocean, whereas over 80% is reflected at the Antarctic Ice Sheet, maintaining the strong meridional structure to Southern Hemisphere climate. Over the Southern Ocean, observed cloudiness is extensive limiting the shortwave radiation that reaches the surface. However, the Coupled Model Intercomparison Project version 3 (CMIP3) models were found to simulate excessive absorbed shortwave radiation at the top of the atmosphere in these latitudes, implying excessive incident shortwave radiation at the ocean surface (Trenberth and Fasullo 2010). The modeled representation of clouds were implicated as a leading factor. For ACCIMA, summer-average shortwave radiation (Fig. 6a) is large at the model boundaries and over interior Antarctica and lower between (45-60°S) due to persistent cloudiness over the extratropical ocean, especially over the Pacific and Indian Oceans. At polar latitudes, more shortwave radiation occurs over the Atlantic sector compared to the Pacific.

In contrast, the annual-average incident longwave radiation (Fig. 6b) is zonally symmetric with the minimum (less than 100 W m^{-2}) shifted to the high plateau of East Antarctica. Downward flux at the coast is typically 200 W m^{-2} and increases to about 300 W m^{-2} at 60°S. Even though cloudiness should be greatest over the ocean storm tracks, the incident longwave radiation generally increases north of the storm track. Absorbed shortwave radiation and outgoing longwave radiation at the top of model atmosphere (not shown) are similar to earlier satellite-based estimates (e.g., Briegleb and Bromwich 1998b). Incident radiation fields can also be compared to ERA-I; however, the accuracy of these fields over the Southern Ocean is unknown. Recent comparison of ERA-I to Arctic stations, however, typically show small negative biases for longwave radiation and summer shortwave radiation (Aaron Wilson, personal communication 2014).

The ACCIMA – ERA-I difference for various surface fluxes (Fig. 7) illustrates the important differences between these models. South of 55°S, ACCIMA summer incident shortwave radiation is 10-20 W m^{-2} larger than that of ERA-I, while annual-average longwave radiation has much smaller positive differences. Thus, the simulated incident shortwave may be too large in approximately the same latitudes where Trenberth and Fasullo (2010) noted a positive absorbed shortwave bias for global models. The increased incident shortwave radiation in ACCIMA will be mostly reflected over the Antarctic Ice Sheet and sea ice, but is likely to be important for the summer open-ocean. Annual average sensible heat flux (Fig 8a) is generally negative (heat flux from the atmosphere to the ice surface) over Antarctica, moderately positive (20 W m^{-2}) over the open-ocean, and largest over the mid-latitude continents (60 W m^{-2}). The annual-average latent heat flux (Fig. 8b) is negative or near zero over Antarctica, moderately positive in the regions of seasonal sea ice, and larger than the sensible heat flux (40-60 Wm^{-2}) in regions of year-round open ocean. In comparison to ERA-I, the latent and sensible fluxes are just slightly larger (0-5 W m^{-2}) over Antarctic latitudes in ACCIMA (Fig. 7). They tend to be 5-10 W m^{-2} larger over the Southern Ocean, perhaps in balance with larger incident shortwave and longwave radiation in ACCIMA. The ocean is thus a source of heat to the atmosphere almost everywhere and the land is a small heat sink for the atmosphere. In summary, the atmospheric fields for the ACCIMA coupled-model simulation during years 1999-2010 display realistic atmospheric behavior.

b. Ocean

There are a number of observational constrained diagnostics that indicate that the ocean model for this domain is behaving realistically. These include sea surface temperature (SST), volume transport at Drake Passage, location of ACC fronts, surface kinetic energy, temperature structure and volumes of water in different temperature and salinity classes. The SST averaged over 1999-2010 has the expected zonal pattern (Fig. 9) with latitudinal excursions due to the underlying flow and cold temperatures in the polar gyres in the Ross and Weddell Seas.

The volume transport of the ACC at Drake Passage is a diagnostic of the wind forcing and stratification. The observed transport (Cunningham et al. 2003) is estimated to be 134 ± 11 Sv (1 Sv = 10^6 m^3 s^{-1}). For this model simulation, the transport is higher than observed (a mean of about 170 Sv, Fig. 10), but excess ACC transport is a persistent problem in coarse resolution ocean models (Meijers et al. 2012). There is an increasing trend in the transport in the first 5 years which could be due to adjustment to initial conditions.

Another stiff diagnostic of the Southern Ocean is the location of the frontal jets that are an integral part of the ACC. The mean sea surface height (SSH) is a good proxy for the steady streamfunction for the Southern Ocean. The historical location of ACC fronts (Orsi et al. 1995) are used to calculate an average SSH value for each front (Sallée et al. 2008). Those heights are compared to historical front locations (Fig. 11). The ACC is well simulated in the Amundsen and Bellingshausen Seas where its southern boundary, which is associated with the surfacing of the warm UCDW, is next to the shelf break allowing warm water access to the shelf and the base of the ice shelves. The agreement between model and observations is good except in the Indian

Ocean sector (near Kerguelen Plateau) where the southern boundary extends too far to the south and there are some differences between the location of the Polar front.

The model surface kinetic energy (KE) can be compared to estimates obtained from surface speed estimates from satellite observations of surface elevation (AVISO, Volkov and Pujol 2012 or www.aviso.oceanob.com/duacs) and the use of geostrophy. Mean surface KE (figure not shown) matches well in location and is close in magnitude, as is expected from the mean SSH (Fig. 11). The surface eddy kinetic energy (EKE) is calculated in the model from the difference of the surface flow at each grid point from the monthly mean surface flow, and then averaged over the 12 year simulation. The EKE peak values (figure not shown) are about one fifth of the estimated values, and the area of higher EKE is smaller in the model. This result is not too surprising given the 20 km grid spacing in the ocean model (Hallberg and Gnanadesikan 2006) as well as the fact that the model simulation only saves monthly mean results. Both of these factors will cause model surface EKE to be smaller than observations.

A volumetric TS analysis reveals the volume of water in different ranges of temperature (T) and salinity (S). T classes are between -3°C and 10°C with intervals of 0.1°C, while S classes range from 33 to 35 in steps of 0.01 PSU. This resolution for the TS analysis is comparable to the global analysis by Worthington (1981).

The TS census is calculated from the monthly averaged model solution at the beginning of the simulation (January 1999) and at the end of the simulation (January 2010) for the Antarctic water masses (T and S ranges, Fig. 12a,b). The CSIRO Atlas of Regional Seas (CARS) climatology (Ridgeway et al. 2002, www.cmar.csiro.au/cars/) is used to compare to these ocean results. The volumetric census for the CARS climatology (Fig. 12c) has the general character as those from the model with two differences that stand out. There is considerably more near-freezing water in the model compared to the climatology, and this water is saltier than observed. In addition, there is abundant water around -0.5°C with salinity above 34.7 which is not observed. The difference between the model and CARS census at the beginning of the simulation (January 1999) shows that the model is too salty by 0.1 PSU at temperatures above 3°C (figure not shown). At temperatures below 2°C, the surface water is a bit fresh and the deeper water is a bit salty (by 0.05 PSU). The implication is that deep and bottom waters in the model are a bit salty. This difference remains unchanged throughout the 12 year simulation (figure not shown).

Two vertical temperature sections are chosen for comparison between the model and CARS. The 30°E section (Fig. 13) extends through the Weddell Sea where dense water is formed (a cold-water shelf) while the 135°W section (Fig. 14) is through the Bellingshausen Sea where warm water intrudes onto the shelf (a warm-water shelf). The differences at 30°E section are clearest near the bottom at 60°S where the bottom water is colder than observed. It is also saltier and hence denser. This difference is traced to the shelf where excess freezing on the shelf is liberating too much salt. A contributing factor could be that the water that cascades from the shelf does not mix sufficiently as it moves down the continental slope. Similar difficulties with excessive cooling on Antarctic shelves and too-salty Antarctic Bottom Water occur in coupled climate models (Danabasoglu et al. 2012) due to the delicate balance of ocean, atmosphere and sea-ice exchanges.

The model sections at 135°W compare better to the CARS climatology (Fig. 14). The initial temperature structure (Fig. 14a) matches well with the climatology (Fig. 14c) although the warm water (UCDW) at 500 m depth is eroded in the model. By the end of the simulation (Fig. 14b), the intruding UCDW (500 m depth south of 60°S) is reduced but the remainder of the temperature structure is comparable to the climatology.

The total heat content over the continental shelf is a diagnostic for the potential to melt ice shelves (since ice shelves are not explicitly included in the model). Antarctic shelf areas are defined (for this calculation) as places that are less than 630 m deep and south of 60°S. For each of these locations and for each month, the total heat content is obtained by vertically integrating the heat content above surface freezing (T = -1.88°C) between 105 m depth and the bottom. These values of integrated heat content are average over 10° longitude bins around the Antarctic continent (Fig. 15).

Over most of the Antarctic coast between 0° and 160°E longitudes, there is a clear seasonal change in heat content (Fig. 15), driven by surface heating and cooling along with deeper mixed layers or vertical convection. Between 180° and 300°E longitude, the presence of warm water on the shelf is evident in the increased heat content, with the warmest conditions in the Bellingshausen Sea (250 to 280°E). Over the 12 years of this simulation, the heat content on the shelf declines, but there is no trend in the ocean surface heat flux. A possible explanation for this loss of heat is that the ocean loses more heat to the atmosphere in the winter than is replaced by sufficient exchange of warm water (CDW). A second possibility is that the water that is being exchanged onto the Antarctic shelves is colder than it should be, and so it flushes the warm water from the shelf. The temperature section at 135°W (Fig. 14) has water near the shelf break that is as much a 1°C colder than should be according to the climatology (particularly towards the end of the simulation).

The SST is an important driver of atmospheric dynamics so it is important to compare the model SST to observations. The CARS climatology provides one estimate of SST, although for a single time which misses the seasonal cycle expected for high southern latitudes. The difference in model SST from CARS is calculated at every model saved time (monthly). The pattern of difference for each month (figures not shown) have similar patterns with positive differences from 70^{o}S to 60^{o}S and negative differences north of 55^{o}S and along the Antarctic coastal areas. There is no change in the SST difference over the span of the simulation. A mean across all months (figure not shown) is a compact way to see this pattern and compensates for the missing seasonal variability in CARS. The model SST is about 0.5^{o}C too cold north of the ACC and about the same amount too warm over the ACC. Surface temperature in coastal areas is about correct in the mean.

Some coupled global simulations (CCSM4, for example) have oceans with lower than observed temperatures (Danabasoglu et al. 2012) which are attributed to excess heat loss through the upper atmosphere. In this Southern Ocean model, the differences in surface temperature are attributable to biases in the atmospheric radiation through inaccuracies of simulated cloud properties. Excess or insufficient incident radiation leads to warmer or colder SST. Bottom water in the model is too cold (Fig. 13) which is due to excess heat loss on the Antarctic shelves.

c. Sea Ice

The sea ice climatology and variability provide a stiff test of the coupled system, depending critically on accurate simulation of the oceanic stratification and atmospheric temperature and precipitation, which are not well constrained by the lateral boundary conditions or nudging of the upper atmosphere. The simulated March minimum and September maximum in sea-ice concentration (Fig. 16) compare well to National Snow and Ice Data Center (NSIDC, Fetterer et al. 2002) composites based on satellite microwave measurements. Sea ice extent, the area of sea ice with concentration greater than 15%, also compares well to model results (Fig. 17) with the growth and decay of sea ice being well represented. The seasonal and interannual progression of total sea-ice extent is accurately represented, but there is a low bias during the summer months. The maximum sea ice extent matches observations to within 2 million square km or less (about 10%), most of the error being a matter of timing (Fig. 17b), as the model develops ice slightly later than indicated by observations. The minimum sea ice extent in the model has too little ice by about 2 million square km which is about half of the sea ice extent at minimum (Fig. 17b), and this could be due to the excess summer surface shortwave radiation.

In summary, the coupled model system accurately reproduces the climatology and variability of the observed Antarctic climate system. The large domain allows for a fully coupled simulation of the entire Southern Ocean, as in global climate models, but with the fine scale structure of limited area models needed to ultimately simulate basal melt rates.

3. Discussion

The ultimate focus of the ACCIMA project is on heat delivered to Antarctic ice shelves which lead to changes in basal melt. Because this model does not have active ice shelves, we calculate the heat content of ocean water on these continental shelves and analyze how this heat content changes. The heat content varies considerably in different regions (Fig. 15), and primarily reflects the temperature of the ocean water offshore of the shelf break which is able to intrude onto the shelf. The warm shelf areas in the model have decreased heat content (Fig. 15).

There are two mechanisms that remove heat from the shelf: Exchange with the atmosphere and exchange with the offshore ocean. Without doing a detailed heat budget, the following analysis indicates that the major exchange mechanism depends on the atmosphere. The total heat content in the ocean over the continental shelves is calculated. The shelf areas are identified as before as areas south of 60^{o}S no deeper than 630 m. The total heat content (J m^{-2}) of the shelf is calculated (integrated from the surface to the bottom) for each month and averaged over all shelf grids. The change in heat content between each month is the heat flux (W m^{-2}) required to accomplish the change. The monthly average surface heat flux between the ocean and atmosphere is available in the model output.

The heat exchange with the atmosphere is very close to the change in heat content (Fig. 18) indicating that the atmosphere (and surface radiation fluxes) are the major process accounting for the ocean temperature change over the shelf. During the summer months, the surface flux accounts for ¾ or more of the observed heat content change. In the winter, there is more surface flux (loss) than observed heat change, although the differences are not large. The difference (red line in Fig. 18) in the surface heat flux and the monthly heat content change is an estimate of the average heat flux across the shelf break. The mean heat flux is about 25 W m^{-2}; there is no trend in this flux across the 12 years of simulation.

4. Summary and Conclusions

The ACCIMA project has developed a regional coupled atmosphere/ocean/land/sea ice model that is applied to the Southern Ocean and continental Antarctica. The motivation for the study is the need to understand the mass balance of the ice sheet and floating ice shelves of Antarctica, a critical input to projections of global sea-level change. Mesoscale processes acting in the ocean, atmosphere, and on land, which are not directly represented in most climate models, are known to be important in heat exchange at polar latitudes. The grid spacing of the ACCIMA model (60 km for the atmosphere and land, and 20 km for the ocean and sea ice) is smaller than is used in typical coupled climate simulations to better represent regional physical processes.

Coupled simulations have been run for 1999-2010 driven by the ERA-I global atmospheric reanalysis and climatological conditions around the northern boundary of the ocean. The atmosphere model develops very realistic wind patterns over the continent and near the Antarctic coast in response to land topography. SST develops a realistic pattern compared to observations but tends to be a bit warm in the south and cold in the north, perhaps due to biases in the surface radiation fluxes. Sea ice is well represented in both timing and coverage in the model but has a somewhat low ice extent during the summer, possibly linked to excessive incident shortwave radiation. Ocean circulation and water characteristics compare well with observations. Heat content over the Antarctic shelves, which is one major source of glacial melt, has a realistic pattern but declines over the 12 years of the simulation. Further investigation is required to isolate the cause. The main focus of the ACCIMA project is to better understand heat transport onto the continental shelves. We are now pursuing coupled simulations with a higher resolution ocean (10 km grid spacing) and atmosphere (20 km) to improve the realism of the simulation and better capture mesoscale processes in both the atmosphere and ocean. Preliminary results suggest a significant improvement in ocean EKE in particular, as expected. Additional physics enhancements, especially for cloud processes, are desirable and are being pursued. A more detailed analysis of the role of the atmosphere and ocean in transporting heat onto the continental shelf is also planned, with additional focus on the vertical structure of heat transport. In particular, basal melt at the grounding line depends on the heat transport at depth.

Acknowledgments. This research is supported by NSF Grants ANT-1048989, ANT-1049081, and ANT-1049089. We gratefully appreciate this support. We would like to acknowledge the use of computational resources (ark:/85065/d7wd3xhc) at the NCAR-Wyoming Supercomputing Center provided by the National Science Foundation and the State of Wyoming, and supported by NCAR's Computational and Information Systems Laboratory. We thank Tony Craig and John Cassano for supplying the RASM code and helpful comments. Altimeter products were produced by Ssalto/Duacs and distributed by AVISO, with support of CNES (www.aviso.oceanobs.com/duacs/). We also thank Ruby Leung for helpful comments.

References

Bitz, C.M., and W.H. Lipscomb, 1999: An energy-conserving thermodynamic model of sea ice. *J. Geophys. Res.*, **104**, 15,669-15,678, doi:10.1029/1999JC900100.

Briegleb, B.P., and D.H. Bromwich, 1998a: Polar climate simulation of the NCAR CCM3. *J. Climate*, **11**, 1270-1286, doi:10.1175/1520-0442.

Briegleb, B.P., and D.H. Bromwich, 1998b: Polar radiation budgets of the NCAR CCM3. *J. Climate*, **11**, 1246-1269, doi:10.1175/1520-0442.

Briegleb, B.P., G. Danabasoglu, and W.G. Large, 2010: An overflow parameterization for the ocean component of the Community Climate System Model. *NCAR Tech. Note NCAR/TN-481+STR*, 72 pp.

Bromwich, D.H., T.R. Parish, A. Pellegrini, C.R. Stearns, and G.A. Weidner, 1993: Spatial and temporal variations of the intense katabatic winds at Terra Nova Bay, Antarctica. In Antarctic Meteorology and Climatology: Studies Based on Automatic Weather Stations, *Antarctic Research Series*, **61**, edited by D. H. Bromwich and C. R. Stearns, Amer. Geophys. Union, 47-68.

Bromwich, D.H., K.M. Hines, and L.-S. Bai, 2009: Development and testing of Polar WRF. 2. Arctic Ocean. *J. Geophys. Res.*, **114,** D08122, doi:10.1029/2008JD010300.

Bromwich, D.H., J.P. Nicolas, and A.J. Monaghan, 2011: An assessment of precipitation changes over Antarctica and the Southern Ocean since 1989 in contemporary global reanalyses. *J. Climate*, **24**, 4189-4209, doi:10.1175/2011JCLI4074.1.

Bromwich, D.H., J.P. Nicolas, A.J. Monaghan, M.A. Lazzara, L.M. Keller, G.A. Weidner, and A.B. Wilson, 2013a: Central West Antarctica among the most rapidly warming regions on Earth. *Nature Geoscience*, **6**, 139-145, doi: 10.1038/ngeo1671.

Bromwich, D.H., F.O. Otieno, K.M. Hines, K.W. Manning, and E. Shilo, 2013b: Comprehensive evaluation of polar weather research and forecasting performance in the Antarctic. *J. Geophys. Res.*, **118**, 274-292, doi:10.1029/2012JD018139.

Bryan, K., 1989: The Design of Numerical Models of the Ocean Circulation. In *Ocean Circulation Models: Combining Data and Dynamics*, Kluwer Academic Publishers, pp. 465-500.

Carvajal, G.K., A.K. Wåhlin, L.E.B. Eriksson, and L.M.H. Ulander, 2013: Correlation between Synthetic Aperture Radar surface winds and deep water velocity in the Amundsen Sea, Antarctica. *Remote Sens.*, **5**, 4088-4106, doi:10.3390/rs5084088.

Cassano, J.J., M.E. Higgins, and M.W. Seefeldt, 2011: Performance of the Weather Research and Forecasting (WRF) model for month-long pan-Arctic simulations. *Mon. Wea. Rev.*, **139**, 3469-3488, doi:10.1175/MWR-D-10-05065.1.

Chen, J.L., C.R. Wilson, D. Blakenship, and B.D. Tapley, 2009: Accelerated Antarctic ice loss from satellite gravity measurements. *Nature Geoscience*, **2**, 859-862, doi:10.1038/ngeo694.

Craig, A.P., M. Vertenstein, and R. Jacob, 2012: A new flexible coupler for earth system modeling developed for CCSM4 and CESM1. *Int. J. High Perf. Computing Appl.*, **26,** doi:10.1177/109434201142814.

Cunningham, S.A., S.G. Alderson, B.A. King, and M.A. Brandon, 2003: Transport and variability of the Antarctic Circumpolar Current in Drake Passage. *J. Geophys. Res.*, **108**, 8084, doi:10.1029/2001JC001147.

Danabasoglu, G., S.C. Bates, B.P. Briegleb, S.R. Jayne, M. Jochum, W.G. Large, S. Peacock, and S.G. Yeager, 2012: The CCSM4 ocean component. *J. Climate*, **25,** 1361-1389, http://dx.doi.org/10.1175/JCLI-D-11-00091.1.

DeAngelis, H., and P. Skvarca, 2003: Glacier surge after ice shelf collapse. *Science*, **299**, 1560-1562.

Dee, D.P., and Coauthors, 2011: The ERA-Interim reanalysis: Configuration and performance of the data assimilation system. *Quart. J. R. Meteorol. Soc.*, **137,** 553-597, doi:10.1002/qj.828.

Depoorter, M.A., J.L. Bamber, J.A. Griggs, J.T.M. Lenaerts, S.R.M. Ligtenberg, M.R. van den Broeke, and G. Moholdt, 2013: Calving fluxes and basal melt rates of Antarctic ice shelves. *Nature*, **502,** 89-92, doi:10.1038/nature12567.

Dinniman, M.S., J.M. Klinck, and W.O. Smith, Jr., 2011. A model study of Circumpolar Deep Water on the West Antarctic Peninsula and Ross Sea continental shelves. *Deep-Sea Research II*, **58,** 1508–1523.

Dinniman, M., J. Klinck, L.-S. Bai, D. Bromwich, and D. Holland, 2014: The effect of atmospheric forcing resolution on the delivery of heat to the Antarctic floating ice shelves. *J. Climate*, in review.

Dupont, T., and R.B. Alley, 2005: Assessment of the importance of ice-shelf buttressing to ice-sheet flow. *Geophys. Res. Letts.*, **32,** L04503.

Fetterer, F., K. Knowles, W. Meier, and M. Savoire, 2002: updated daily, Sea Ice Index. Boulder Colorado, USA. National Snow and Ice Data Center. Digital media.

Flanner, M.G., C.S. Zender, J.T. Randerson, and P.J. Rasch, 2007: Present-day climate forcing and response from black carbon in snow. *J. Geophys. Res.*, **112,** D11202, doi:10.1029/2006JD008003.

Fogt, R.L., D.H. Bromwich, and K.M. Hines, 2011: Understanding the SAM influence on the South Pacific ENSO teleconnection. *Clim. Dyn.*, **36,** 1555-1576, doi:10.1007/s00382-010-0905-0.

Glisan, J.M., W.J. Gutowski, J.J. Cassano, and M.E. Higgins, 2013: Effects of spectral nudging in WRF on Arctic temperature and precipitation simulations. *J. Climate*, **26**, 3985-3999. doi:10.1175/JCLI-D-12-00318.1.

Hallberg, R., and A. Gnanadesikan, 2006: The role of eddies in determining the structure and response of the wind-driven Southern Hemisphere overturning: Results from the modeling eddies in the Southern Ocean (MESO) Project. *J. Phys. Oceanogr.*, **36**, 2232-2252, doi: http://dx.doi.org/10.1175/JPO2980.1.

Hellmer, H.H., S.S. Jacobs, and A. Jenkins, 1998: Oceanic erosion of a floating Antarctic glacier in the Amundsen Sea. In: Jacobs, S.S. and Weiss, R.F. (Eds.), *Ocean, Ice, and Atmosphere: Interactions at the Antarctic Continental Margin*, AGU *Ant. Res. Ser.*, Vol. 75, pp. 83-99.

Hines, K.M., and D.H. Bromwich, 2008: Development and testing of Polar WRF. Part I. Greenland Ice Sheet meteorology. *Mon. Wea. Rev.*, **136,** 1971-1989.

Hines, K.M., D.H. Bromwich, M. Barlage, and A.S. Slater, 2011: Development and testing of Polar WRF. Part III. Arctic Land. *J. Climate*, **24,** 26-48, doi:10.1175/2010JCLI3460.1.

Holland, P.R., A. Jenkins, and D.M. Holland, 2010: Ice and ocean processes in the Bellingshausen Sea, Antarctica. *J. Geophys. Res.*, **115**, C05020, doi:10.1029/2008JC005219.

Holland, M.M., D.A. Bailey, B.P. Briegleb, B. Light, and E. Hunke, 2012: Improved Sea Ice Shortwave Radiation Physics in CCSM4: The Impact of Melt Ponds and Aerosols on Arctic Sea Ice. *J. Climate*, **25**, 1413–1430, doi: dx.doi.org/10.1175/JCLI-D-11-00078.1

Hollands, T., V. Haid, W. Dierking, R. Timmermann, and L. Ebner, 2013: Sea ice motion and open water area at the Ronne polynya, Antarctica: Synthetic aperture radar observations versus model results. *J. Geophys. Res.*, **118**, 1-15, doi:10.1002/jgrc.20158.

Hunke, E.C., and J.K. Dukowicz, 1997: An elastic-viscous-plastic model for sea ice dynamics. *J. Phys. Oceanogr*., **27**, 1849-1867.

Hunke, E.C., and W.H. Lipscomb, 2008: CICE: The Los Alamos sea ice model, documentation and software, version 4.0. Los Alamos National Laboratory Tech. Rep. LA-CC-06-012, 76 pp.

Hurrell, J.W., and Coauthors, 2013: The Community Earth System Model: A Framework for Collaborative Research. *Bull. Amer. Meteor. Soc.*, **94,** 1339-1360.

Jacobs, S.S., H.H. Hellmer, C.S.M. Doake, A. Jenkins, and R.M. Frolich, 1992: Melting of ice shelves and the mass balance of Antarctica. *J. Glaciol.*, **38,** 375-387.

Jacobs, S.S., H.H. Hellmer and A. Jenkins, 1996: Antarctic ice sheet melting in the Southeast Pacific. *Geophys. Res. Lett.*, **23,** 957-960.

Jacobs, S., A. Jenkins, H. Hellmer, C. Giulivi, F. Nitsche, B. Huber, and R. Guerrero, 2012: The Amundsen Sea and the Antarctic Ice Sheet. *Oceanography*, **25,** 154-163, doi:10.5670/oceanog.2012.90.

Jenkins, A., D.G. Vaughn, S.S. Jacobs, H.H. Hellmer, and J.R. Keys, 1997: Glaciological and oceanographic evidence of high melt rates beneath Pine Island Glacier, West Antarctica. *J. Glaciol.*, **43**, 114-121.

Jenkins, A., and S.S. Jacobs, 2008: Circulation and melting beneath George VI Ice Shelf, Antarctica. *J. Geophys. Res.*, **113**, C04013, doi:10.1029/2007JC004449.

Johnson, M.A., 1989: Forcing the volume transport through the Drake Passage. *J. Geophys. Res.*, **94**, 16,115-16,124.

Kain, J.S., 2004: The Kain-Fritsch convective parameterization: An update. *J. Appl. Meteor.*, **43,** 170-181.

Kalnay. E., and Coauthors, 1996: The NCEP/NCAR 40-year reanalysis project. *Bull. Amer. Meteor. Soc.*, **77**, 437-471, doi:http://dx.doi.org/10.1175/1520-0477(1996)077<0437;TNYRP>2.0.CO;2.

Large, W., and S. Yeager, 2008: The global climatology of an interannually varying air-sea flux data set. *Clim. Dyn.*, **33,** 341-364, doi:10.1007/s00382-008-0441-3.

Lawrence, D.M., K.W. Oleson, M.G. Flanner, P.E. Thornton, S.C. Swenson, P.J. Lawrence, X. Zeng, Z.-L. Yang, S. Levis, K. Sakaguchi, G.B. Bonan, and A.G. Slater, 2011: Parameterization improvements and functional and structural advances in version 4 of the Community Land Model. *J. Adv. Model. Earth Syst.*, **3,** M03001, doi:10.1029/2011MS000045.

Li, X., D.M. Holland, E.P. Gerber, and C. Yoo, 2014: Impacts of the north and tropical Atlantic Ocean on the Antarctic Peninsula and sea ice. *Nature*, **505,** 538-542, doi:10.1038/nature12945.

Liang, X., D.P. Lettenmaier, E.F. Wood, and S.J. Burges, 1994: A Simple hydrologically Based Model of Land Surface Water and Energy Fluxes for GCMs. *J. Geophys. Res.*, **99**, 14,415-14,428.

Lipscomb, W.H., and E.C. Hunke, 2004: Modeling sea ice transport using incremental remapping. *Mon. Wea. Rev*, **132**, 1341-1354.

Maslowski, W., J.C. Kinney, M. Higgins, and A. Roberts, 2012: The future of Arctic sea ice. *Annu. Rev. Earth Planet. Sci.*, **30,** 625-654, doi:10.1146/annurev-earth-042711-105345.

Mathiot, P., N.C. Jourdain, B. Barnier, H.Gallée, J.M. Molines, J. Le Sommer, and T. Penduff, 2012: Sensitivity of coastal polynyas and high-salinity shelf water production in the Ross Sea, Antarctica, to the atmospheric forcing. *Ocean. Dyn.*, **62**, 701-723, doi:10.1007/s10236-012-0521-y.

Meijers, A.J.S., E. Shuckburgh, N. Bruneau, J.-B. Sallee,T.J. Bracegirdle, and Z. Wang, 2012: Representation of the Antarctic Circumpolar Current in the CMIP5 climate models and futures changes under warming scenarios. *J. Geophys. Res.*, **117,** C12008, doi:10.1029/2012JC008412.

Moffat, C., B. Owens, and R.C. Beardsley, 2009: On the characteristics of Circumpolar Deep Water intrusions to the west Antarctic Peninsula continental shelf. *J. Geophys. Res.*, **114**, C05017, doi:10.1029/2008JC004955.

Nakanishi, M., and H. Niino, 2006: An improved Mellor Yamada level 3 model: Its numerical stability and application to a regional prediction of advection fog. *Boundary Layer Meteorology*, **119,** 397-407.

Okumura, Y.M., D. Schneider, C. Deser, and R. Wilson, 2012: Interdecadal climate variability over Antarctica and linkages to the Tropics: Analysis of ice core, instrumental, and tropical proxy data. *J. Climate*, **25,** 7421-7441, doi:http//dx.doi.org/10.1175/JCLI-D-12-00050.1.

Oleson, K.W., and Coauthors, 2010: Technical description of version 4.0 of the Community Land Model (CLM). *NCAR Tech. Note NCAR/TN-478+STR*, 257 pp.

Orsi, A.H., T. Whitworth III, and W.D. Nowlin Jr., 1995: On the meridional extent and fronts of the Antarctic Circumpolar Current. *Deep-Sea Research*, **42**, 641-673.

Overpeck, J.T., B.L. Otto-Bliesner, G.H. Miller, D.R. Muhs, R.B. Alley, and J.T. Kiehl, 2006: Paleoclimatic evidence for future ice-sheet instability and rapid sea-level rise. *Science*, **311**, 1747-1750, doi:10.1126/science.1115159.

Padman, L., D.P. Costa, M.S. Dinniman, H.A. Fricker, M.E. Goebel, L.A. Huckstadt, A. Humbert, I. Joughin, J.T.M. Lenaerts, S.R.M. Ligtenberg, T. Scambos, and M.R. van den Broeke, 2012: Oceanic controls on the mass balance of Wilkins Ice Shelf, Antarctica. *J. Geophys. Res.*, **117,** C01010, doi:10.1029/2011JC007301.

Payne, A.J., A. Vieli, A. Shepherd, D.J. Wingham, and E. Rignot, 2004: Recent dramatic thinning of largest West Antarctic ice stream triggered by oceans. *Geophys. Res. Lett.*, **31**, L23401, doi:10.1029/2004GL021284.

Petrelli, P., N.L. Bindoff, and A. Bergamasco, 2008: The sea ice dynamics of Terra Nova Bay and Ross Ice Shelf Polynyas during a spring and winter simulation. *J. Geophys. Res.*, **113**, C09003, doi:10.1029/2006JC004048.

Potter, J.R., and J.G. Paren, 1985: Interaction between ice shelf and ocean in George VI Sound, Antarctica. In: Jacobs, S.S. (Ed.), *Oceanology of the Antarctic Continental Shelf*, AGU *Ant. Res. Ser.*, **43**, pp. 35-58.

Powers, J., K.W. Manning, D.H. Bromwich, J.J. Cassano, and A M. Cayette, 2012: A decade of Antarctic science support through AMPS. *Bull. Amer. Meteor. Soc.*, **93**, 1699-1712, doi:10.1175/BAMS-D-11-00186.1.

Pritchard, H.D., R.J. Arthern, D.G. Vaughan, and L.A. Edwards, 2009: Extensive dynamic thinning on the margins of the Greenland and Antarctic ice sheets. *Nature*, **461**, 971-975, doi:10.1038/nature08471.

Qian, T., A. Dai, K.E. Trenberth, and K.W. Oleson, 2006: Simulation of global land surface conditions from 1948 to 2004: Part I: Forcing data and evaluations. *J. Hydrometeor.*, **7,** 953-975.

Ridgeway, K.R., J.R. Dunn, and J.L. Wilkin, 2002: Ocean interpolation by four-dimensional least squares-Application to the waters around Australia. *J. Atmos. Ocean. Tech.*, **19,** 1357-1375.

Rignot, E., I. Velicogna, M.R. van den Broeke, A. Monaghan, and J. Lenaerts, 2011: Acceleration of the contribution of the Greenland and Antarctic Ice Sheets to sea level rise. *Geophys. Res. Lett.*, **38,** L05503, doi:10.1029/2011GL046583.

Rignot, E., S. Jacobs, J. Mouginot, and B. Scheuchl, 2013: Ice shelf melting around Antarctica**.** *Science*, **13,** 266-270, doi:10.1126/science.1235798.

Sallée, J.B., K. Speer, and R. Morrow, 2008: Response of the Antarctic Circumpolar Current to Atmospheric Variability. *J. Climate*, **21,** 3020-3039, doi:10.1175/2007JCLI1702.1.

Schoof, C., 2007: Ice sheet grounding line dynamics: steady states, stability and hysteresis. *J. Geophys. Res.*, **112,** F03S28, doi:10.1029/2006JF000664.

Skamarock, W.C., J.B. Klemp, J. Dudhia, D.O. Gill, D.M. Barker, M. Duda, X.-Y. Huang, W. Wang, and J.G. Powers 2008: A Description of the Advanced Research WRF Version 3. *NCAR Tech. Note NCAR/TN–475+STR*, 125 pp.

Smith, R.D., and Coauthors, 2010: The Parallel Ocean Program (POP) reference manual: Ocean component of the Community Climate System Model (CCSM) and Community Earth System Model (CESM). *Los Alamos National Laboratory Tech. Rep. LAUR-10-01853*, 141 pp.[Available online at www.cesm.ucar.edu/models/cesm1.0/pop2/doc/sci/POPRefManual.pdf.]

Steig, E.J., D.P. Schneider, S.D. Rutherford, M.E. Mann, J.C. Comiso, and D.T. Shindell, 2009: Warming of the Antarctic ice-sheet surface since the 1957 International Geophysical Year. *Nature*, **457,** 459-462, doi:10.1038/nature07669.

Steig, E.J., and Coauthors, 2013: Recent climate and ice-sheet changes in West Antarctica compared with the past 2,000 years. *Nature Geoscience*, **6,** 372-375, doi:10.1038/ngeo1778.

Talbot, M.H., 1988: Oceanic environment of George VI Ice Shelf, Antarctic Peninsula. *Annals Glaciol.*, **11**, 161-164.

Tao, W.-K., J. Simpson, and M. McCumber, 1989: An ice-water saturation adjustment. *Mon. Wea. Rev.*, **117,** 231-235.

Thoma, M., A. Jenkins, D. Holland, and S. Jacobs, 2008: Modelling Circumpolar Deep Water intrusions on the Amundsen Sea continental shelf. *Geophys. Res. Lett.*, **35**, L18602, doi:10.1029/2008GL034939.

Thomas, R.E., and Coauthors, 2004: Accelerated sea-level rise from West Antarctica. *Science*, **306**, 255-258, doi:10.1126/science.1099650.

Trenberth, K.T., and J.T. Fasullo, 2010: Simulation of present-day and twenty-first-century energy budgets of the southern oceans. *J. Climate*, **23,** 440-454.

Turner, J., 2004: Review: The El Niño–Southern Oscillation and Antarctica. *Int. J. Climatol.*, **24,** 1–31, doi:10.1002/joc.965

Turner, J., 2007: Polar Meteorology - Understanding Global Impacts. Booklet for World Meteorological Day 2007. WMO, Geneva. 39 pp, WMO-No. 1013, ISBN 92-63-11013-1.

Velicogna, I., 2009: Increasing rates of ice mass loss from the Greenland and Antarctic ice sheets revealed by GRACE. *Geophys. Res. Lett.*, **36**, L19503, doi:10.1029/2009GL040222.

Volkov, D.L., and M.-I. Pujol, 2012: Quality assessment of a satellite altimetry data product in the Nordic, Barents, and Kara seas. *J. Geophys. Res.*, **117,** C03025, doi:10.1029/2011JC007557.

Wåhlin, A.K., O. Kalén, L. Arneborg, G. Björk, G.K. Carvajal, H.K. Ha, T.W. Kim, S.H. Lee, J.H. Lee, and C. Stranne, 2013: Variability of warm deep water inflow in a submarine trough on the Amundsen Sea shelf. *J. Phys. Oceanogr.*, **43**, 2054–2070, doi:10.1175/jpo-d-12-0157.1.

WAIS Divide Project Members, 2013: Onset of deglacial warming in West Antarctica driven by local orbital forcing. *Nature*, doi:10.1038/nature12376.

Walker, D.P., M.A. Brandon, A. Jenkins, J.T. Allen, J.A. Dowdeswell, and J. Evans, 2007: Oceanic heat transport onto the Amundsen Sea shelf through a submarine glacial trough. *Geophys. Res. Lett.*, **34**, L02602, doi:10.1029/2006GL028154.

Wilson, A.B., D.H. Bromwich, and K.M. Hines, 2011: Evaluation of Polar WRF atmospheric and surface processes: An annual simulation. *J. Geophys. Res.*, **116,** D11112, doi:10.1019/2010JD015013.

Wilson, A.B., D.H. Bromwich, and K.M. Hines, 2012: Evaluation of Polar WRF forecasts on the Arctic System Reanalysis domain. 2. Atmospheric hydrologic cycle. *J. Geophys. Res.*, **17**, D04107, doi:10.1029/2011JD016765.

Worthington, L.V., 1981: The water masses of the World Ocean: some results of a fine scale census. In Evolution of Physical Oceanography, B.A. Warren and C. Wunsch (eds), MIT Press, Cambridge, MA, pp 42-69.

Wunsch C., and P. Heimbach, 2007: Practical global ocean state estimation. *Physica D*, **230**, 197-208.

Figure Captions

Figure 1. Model domain. The heavy black line is the outer boundary of the ACCIMA model domain. The colored lines are the historical locations of the ACC fronts (Orsi et al. 1995): Subtropical (outer red), Subantarctic (green), Polar (blue), Southern ACC (cyan), and Southern ACC boundary (inner red) . Green areas are land. The light gray lines are depth contours (1000, 3000 and 5000 m). Geographic locations are indicated by letters; RS=Ross Sea, WS=Weddell Sea, BS=Bellingshausen Sea, AS=Amundsen Sea, PIG=Pine Island Glacier, VL=Victoria Land and WAIS is the West Antarctic Ice Sheet.

Figure 2. Annual mean seal level pressure (hPa) during 1999-2010 for (a) ACCIMA and (b) ERA-Interim (ERA-I). Contour interval is 3 hPa.

Figure 3. ACCIMA average 10-m wind vectors during 1999-2010 for (a) annual average showing the entire domain and (b) winter (June, July and August) average near Antarctica. Color shading is the 2-m air temperature (K). Every 2nd vector is displayed.

Figure 4. Annual-average precipitation (cm) during 1999-2010 for (a) ACCIMA, and (b) ERA-I.

Figure 5. Zonal-mean ACCIMA – ERA-I differences (cm yr^{-1}) for the hydrologic terms precipitation, evaporation/sublimation, and the net difference precipitation minus evaporation during 1999-2010.

Figure 6. Incident radiative fluxes (W m^{-2}) at the surface for (a) summer (DJF) shortwave and (b) annual-average longwave during 1999-2010 for ACCIMA.

Figure 7. Zonal-mean ACCIMA – ERA-I difference fluxes (W m^{-2}) at the surface during 1999-2010 for annual-average sensible and latent heat fluxes and incident annual-average longwave and DJF shortwave radiation.

Figure 8. Annual-mean (a) sensible and (b) latent heat fluxes (W m^{-2}) during 1999-2010 for ACCIMA.

Figure 9. Annual mean sea surface temperature (K) during 2004-2008. Land areas are colored gray.

Figure 10. Volume transport (Sv) at Drake Passage at monthly intervals. Observed value is 134±11Sv (Cunningham et al. 2003).

Figure 11. Mean sea surface height (SSH) over the interval 1999 to 2010. Climatological front locations (blue, Orsi et al. 1995) for the Subantarctic, Polar and southern boundary of the ACC are compared to the best fit SSH contour (red) for each front.

Figure 12. The total volume of water (units of 1000 km^3) for T and S classes with intervals of 0.1°C and 0.01 PSU, respectively, for the ocean. (a) At the beginning of the simulation (January 1999) and (b) at the end of the simulation (January 2010). (c) The CARS climatology for comparison.

Figure 13. Vertical section for temperature at 30°E extending from the continent to 50°S. (a) January 1999, (b) January 2010, and (c) CARS climatology. The contour interval is 0.5°C from -1 to 1°C. Additional contours are at 2, 5 and 9°C.

Figure 14. Vertical section for temperature at 135°W extending from the continent to 50°S. (a) January 1999, (b) January 2010, and (c) CARS climatology. The contour interval is 0.5°C from -1 to 1°C. Additional contours are at 2, 5 and 9°C.

Figure 15. Total heat content for each month for locations south of 60°S with depths less than 635 m over a depth range of 105 m to the bottom. Heat content is integrated over 10° longitude bins.

Figure 16. Sea ice concentration (fraction) for (a) March (lowest coverage) and (b) September (highest coverage) averaged for 1999-2010.

Figure 17. Sea ice extent (total area of ice concentration more than 15%) for each month over the 12 year simulation. (a) Model results are blue; observed (Fetterer et al. 2002) is red. (b) Difference between the model sea ice extent and observations.

Figure 18. Area-averaged surface heat flux (solid line) and heat content change (dashed line) for shelf areas (defined as model cells south of 60°S with depths less than 630 m). The difference (red line) is an estimate of heat exchange across the shelf break.

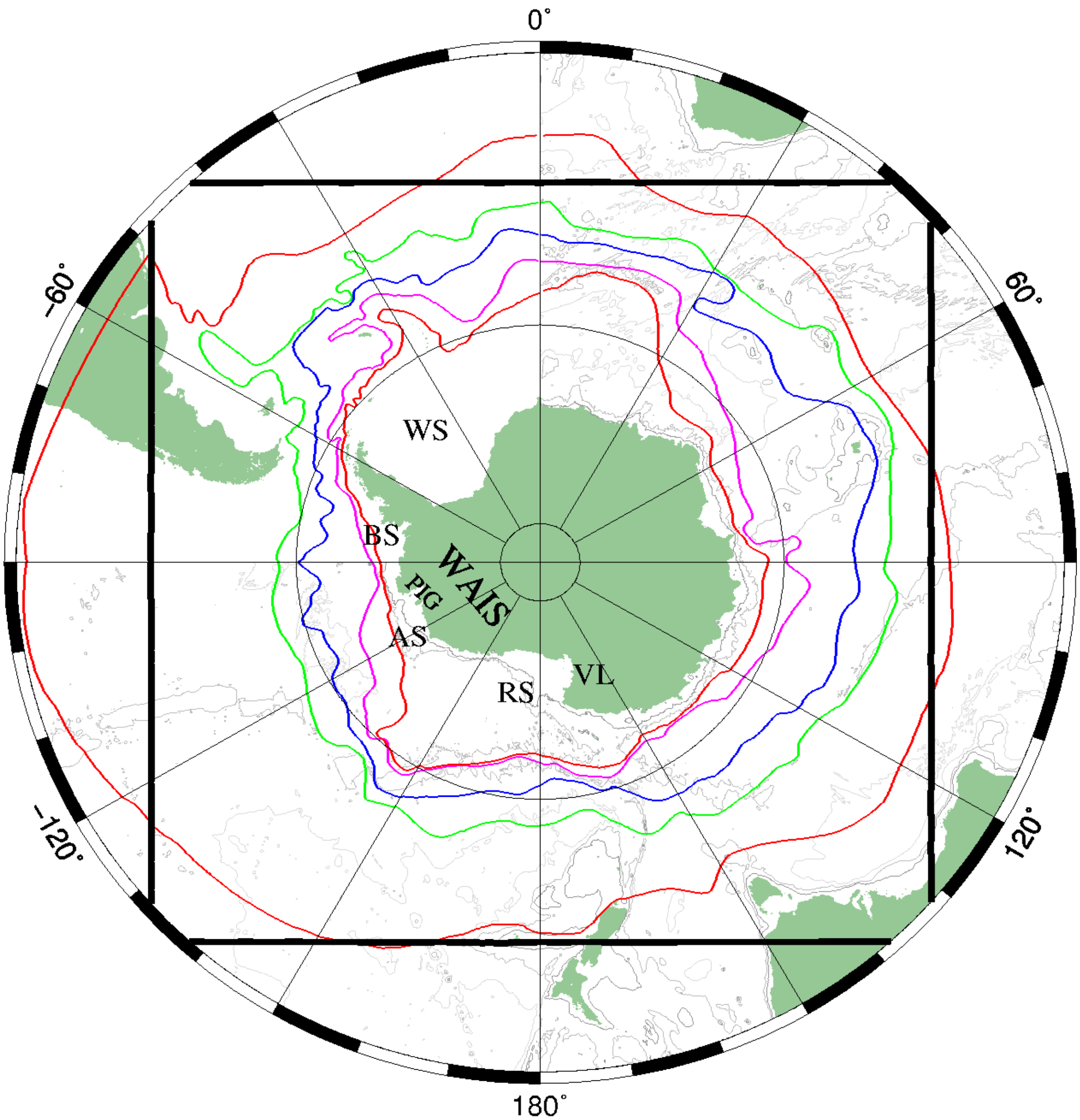

Figure 1. Model domain. The heavy black line is the outer boundary of the ACCIMA model domain. The colored lines are the historical locations of the ACC fronts (Orsi et al. 1995): Subtropical (outer red), Subantarctic (green), Polar (blue), Southern ACC (cyan), and Southern ACC boundary (inner red) . Green areas are land. The light gray lines are depth contours (1000, 3000 and 5000 m). Geographic locations are indicated by letters; RS=Ross Sea, WS=Weddell Sea, BS=Bellingshausen Sea, AS=Amundsen Sea, PIG=Pine Island Glacier, VL=Victoria Land and WAIS is the West Antarctic Ice Sheet.

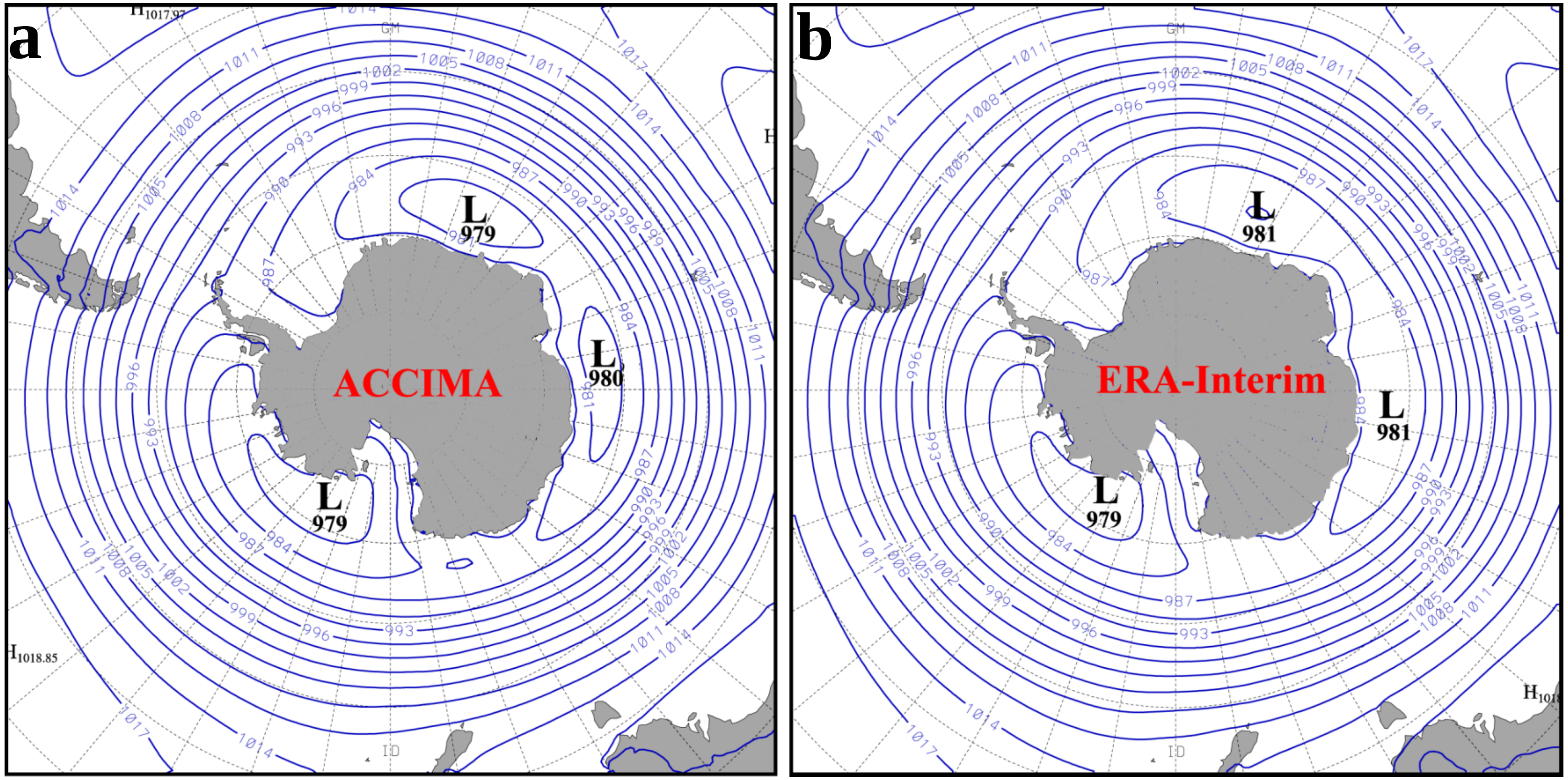

Figure 2. Annual-mean seal level pressure (hPa) during 1999-2010 for (a) ACCIMA and (b) ERA-Interim (ERA-I). Contour interval is 3 hPa.

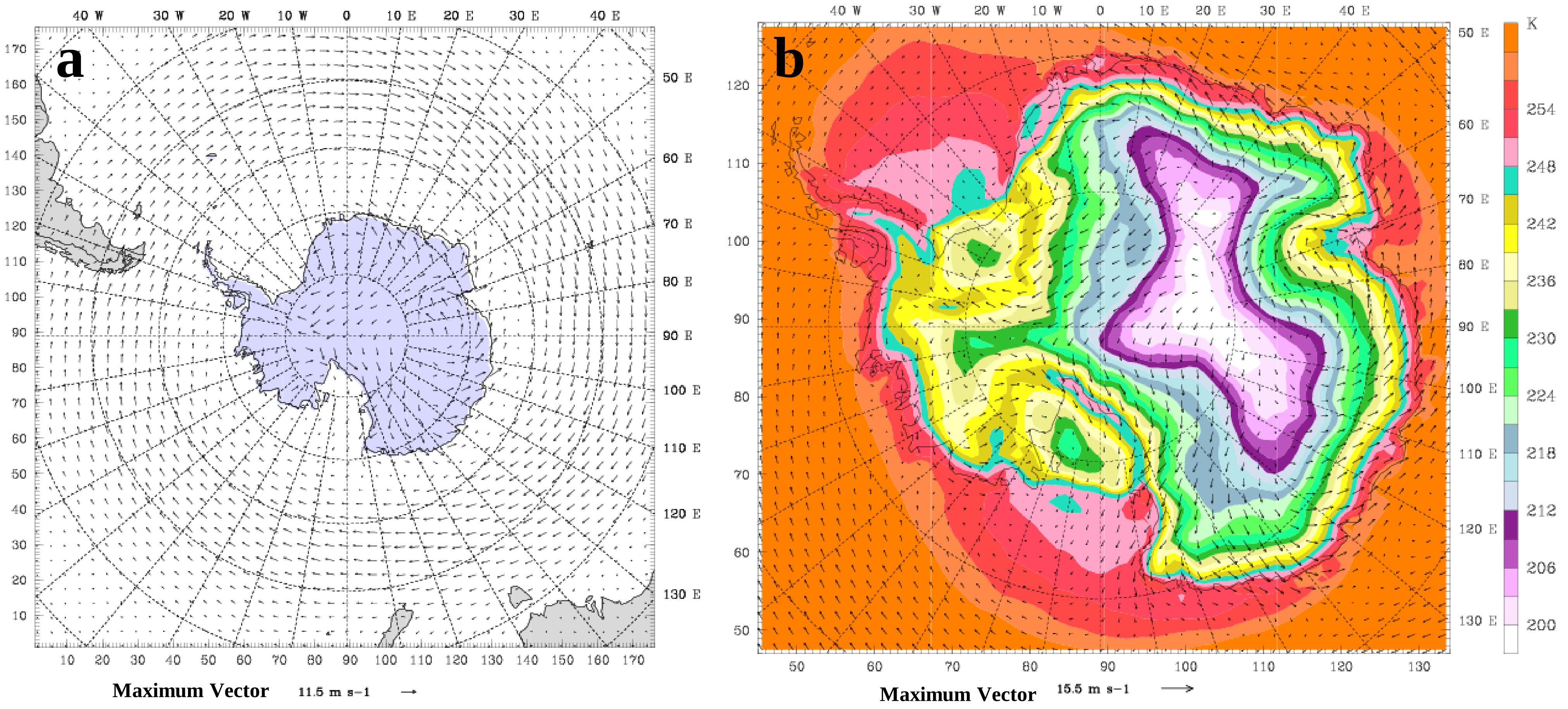

Figure 3. ACCIMA average 10-m wind vectors during 1999-2010 for (a) annual average showing the entire domain and (b) winter (June, July and August) average near Antarctica. Color shading is the 2-m air temperature (K). Every 2nd vector is displayed.

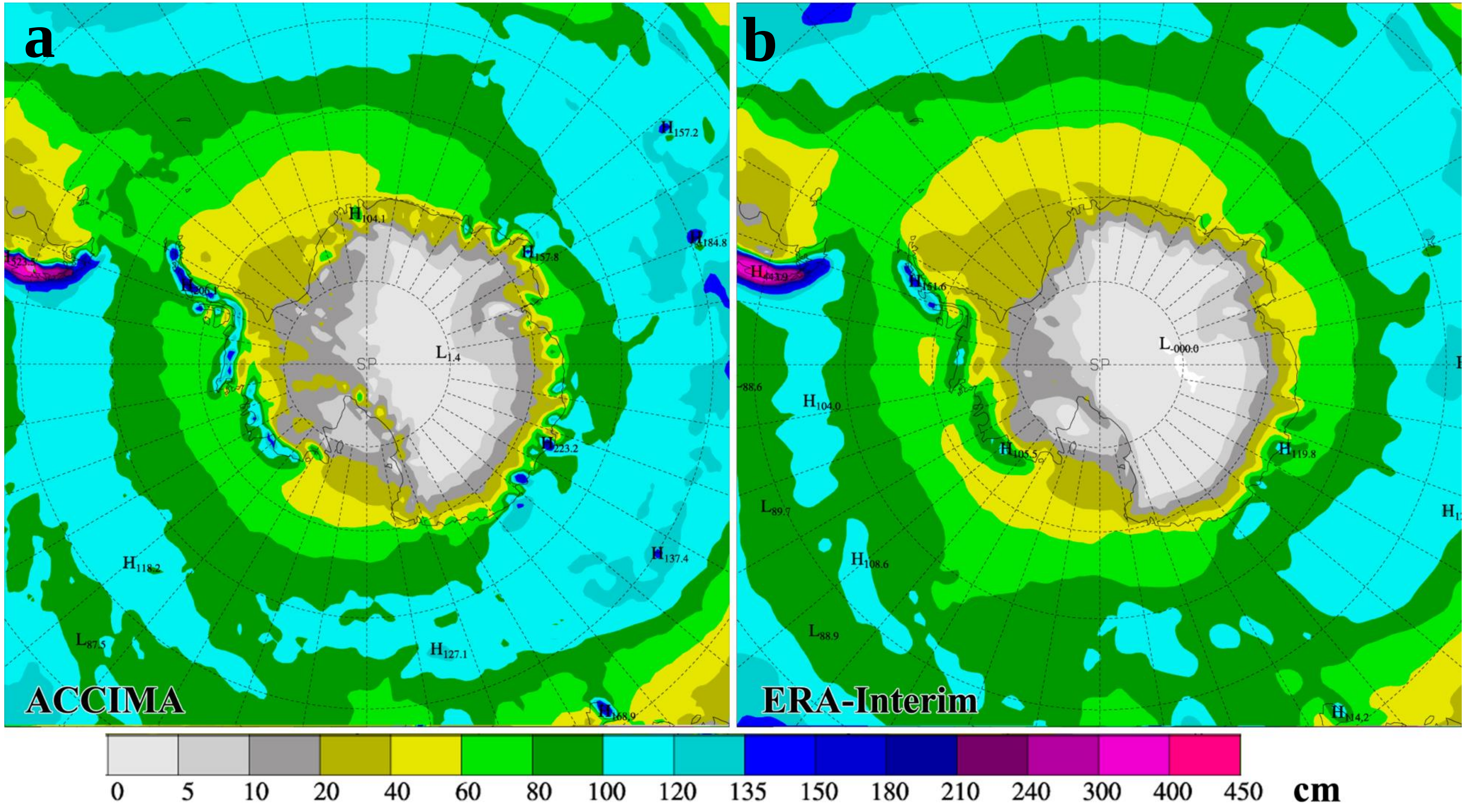

Figure 4. Annual-average precipitation (cm) during 1999-2010 for (a) ACCIMA, and (b) ERA-I.

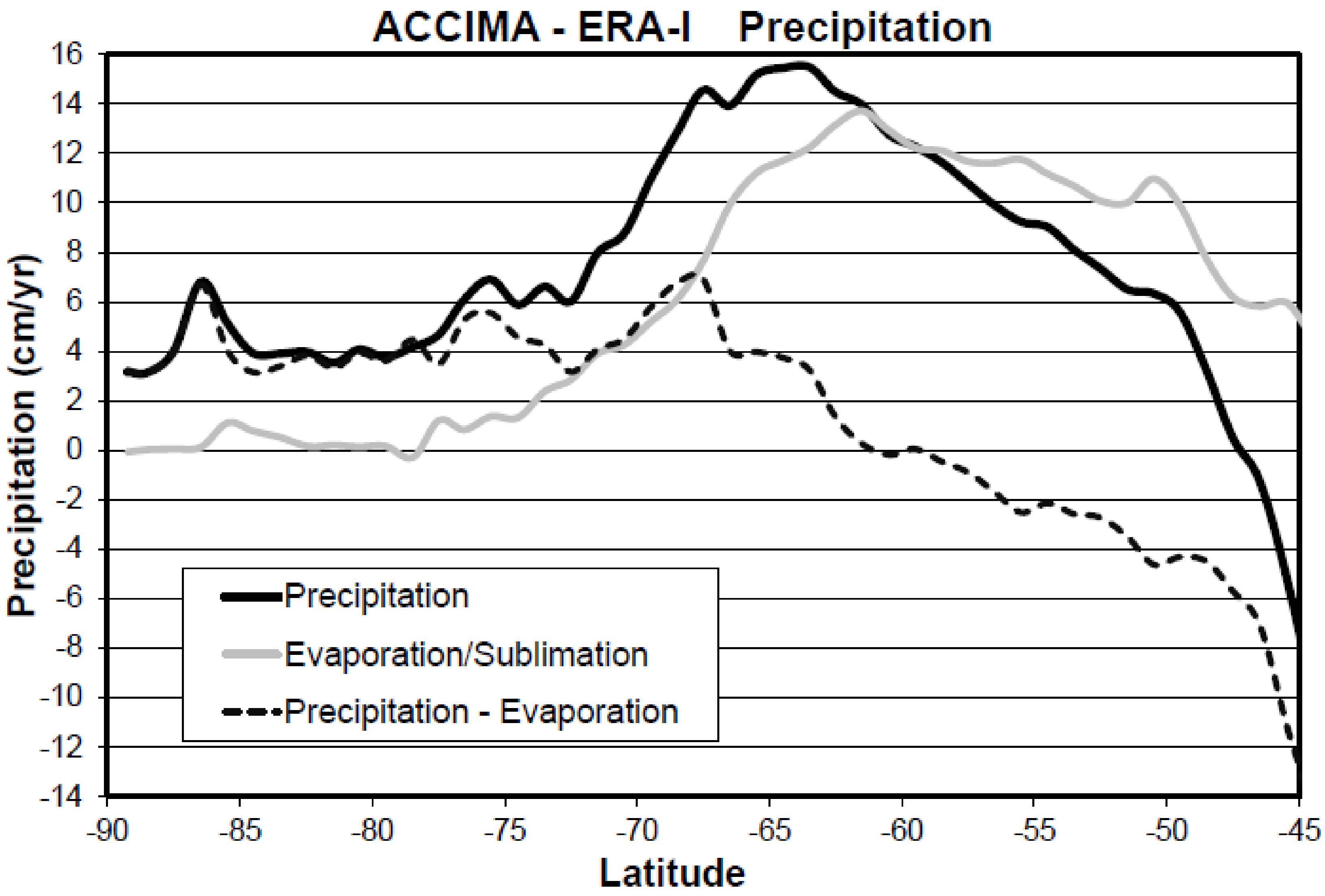

Figure 5. Zonal-mean ACCIMA – ERA-I differences (cm yr^{-1}) for the hydrologic terms precipitation, evaporation/sublimation, and the net difference precipitation minus evaporation during 1999-2010.

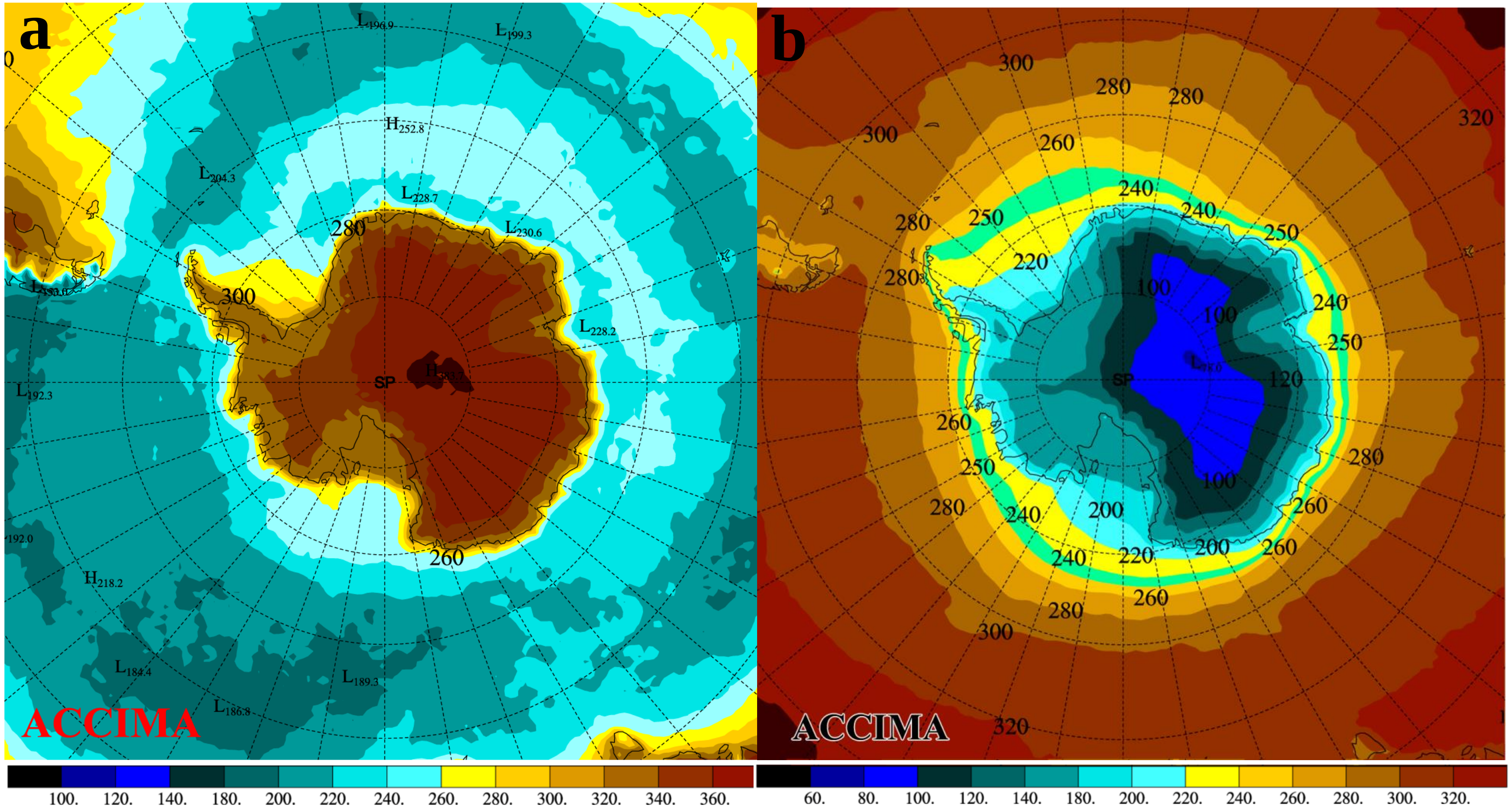

Figure 6. Incident radiative fluxes (W m^{-2}) at the surface for (a) summer (DJF) shortwave and (b) annual-average longwave during 1999-2010 for ACCIMA.

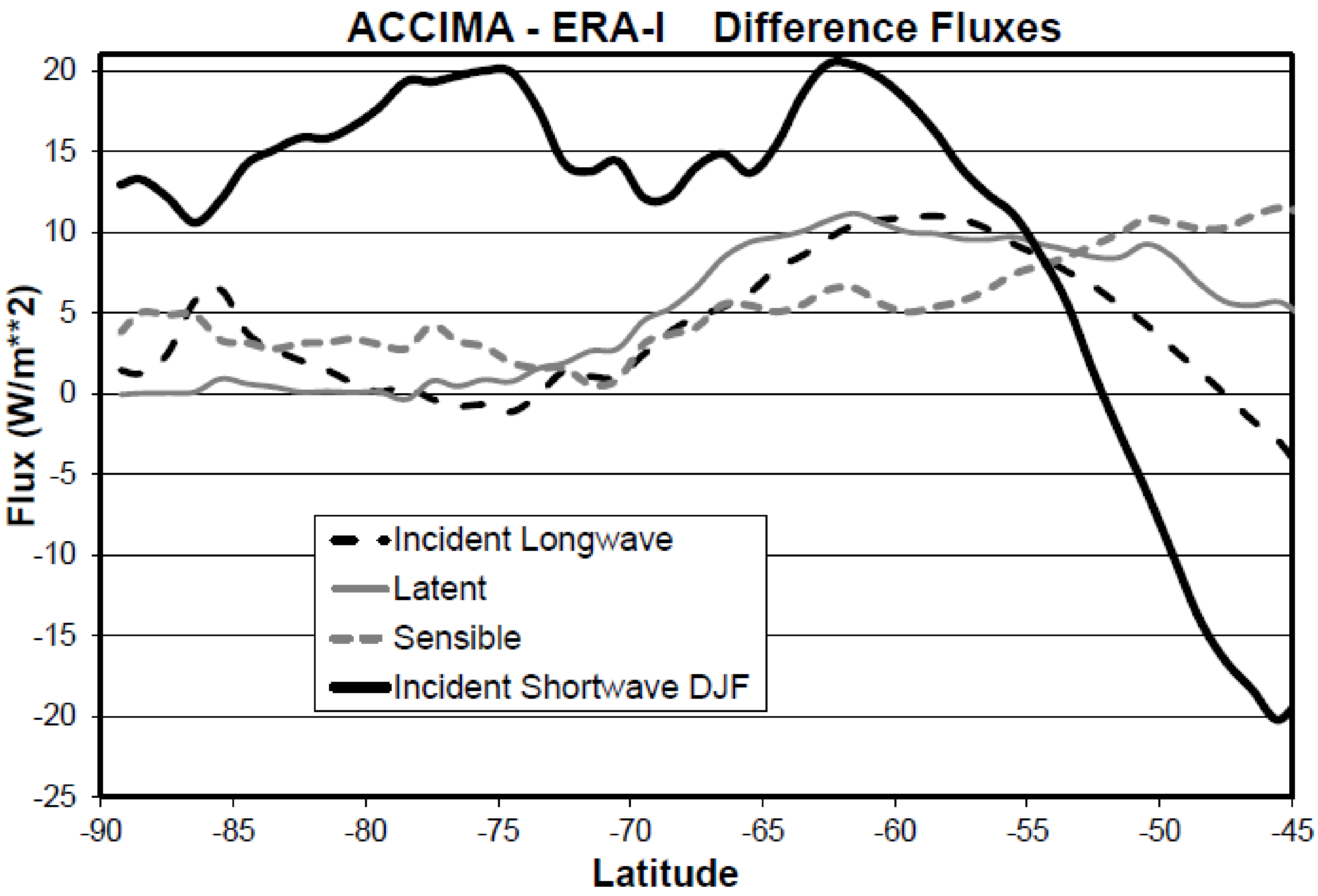

Figure 7. Zonal-mean ACCIMA – ERA-I difference fluxes (W m^{-2}) at the surface during 1999-2010 for annual-average sensible and latent heat fluxes and incident annual-average longwave and DJF shortwave radiation.

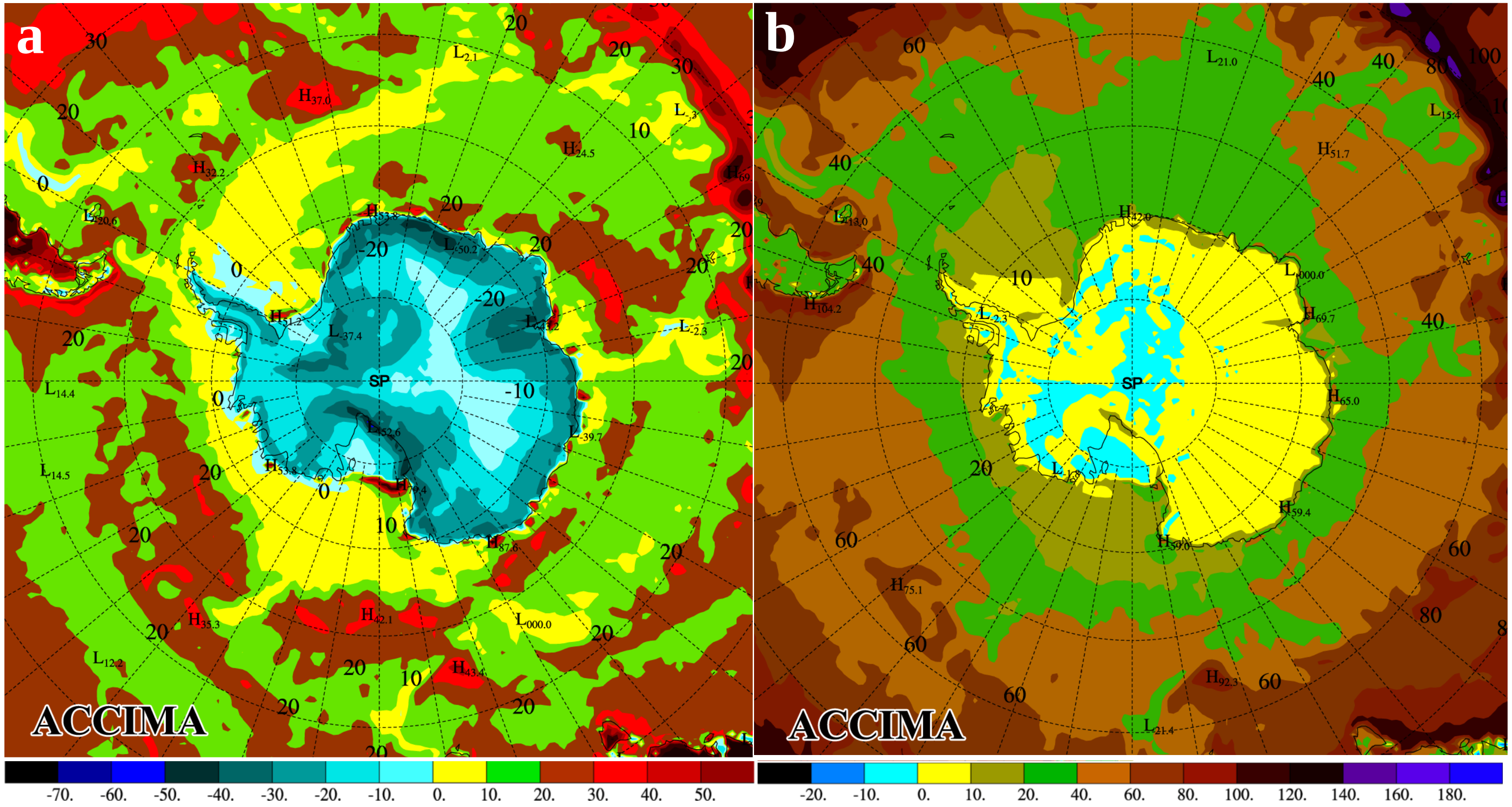

Figure 8. Annual-mean (a) sensible and (b) latent heat fluxes (W m^{-2}) during 1999-2010 for ACCIMA.

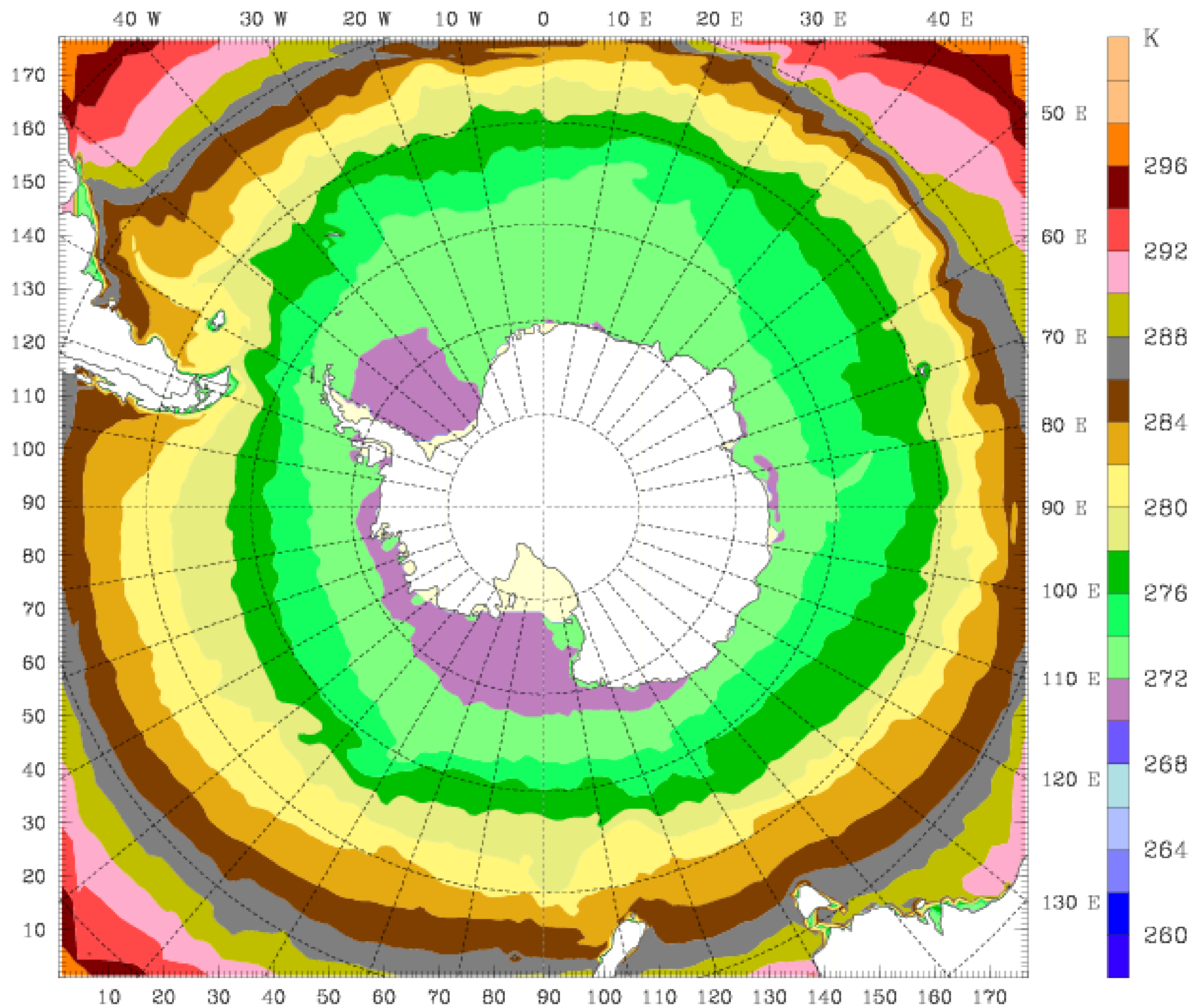

Figure 9. Annual-mean sea surface temperature (K) during 2004-2008. Land areas are colored gray.

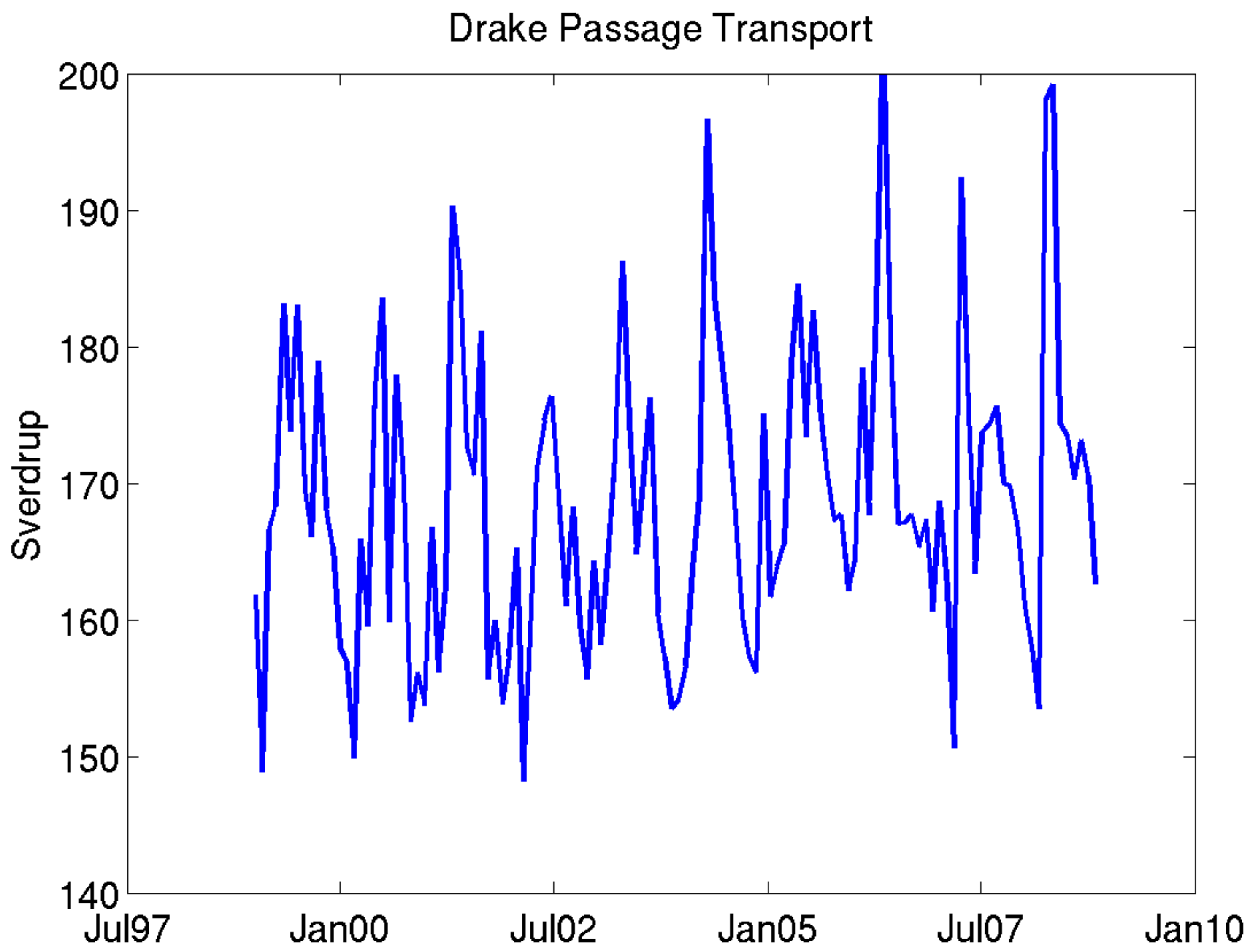

Figure 10. Volume transport (Sv) at Drake Passage at monthly intervals. Observed value is 134±11Sv (Cunningham et al. 2003).

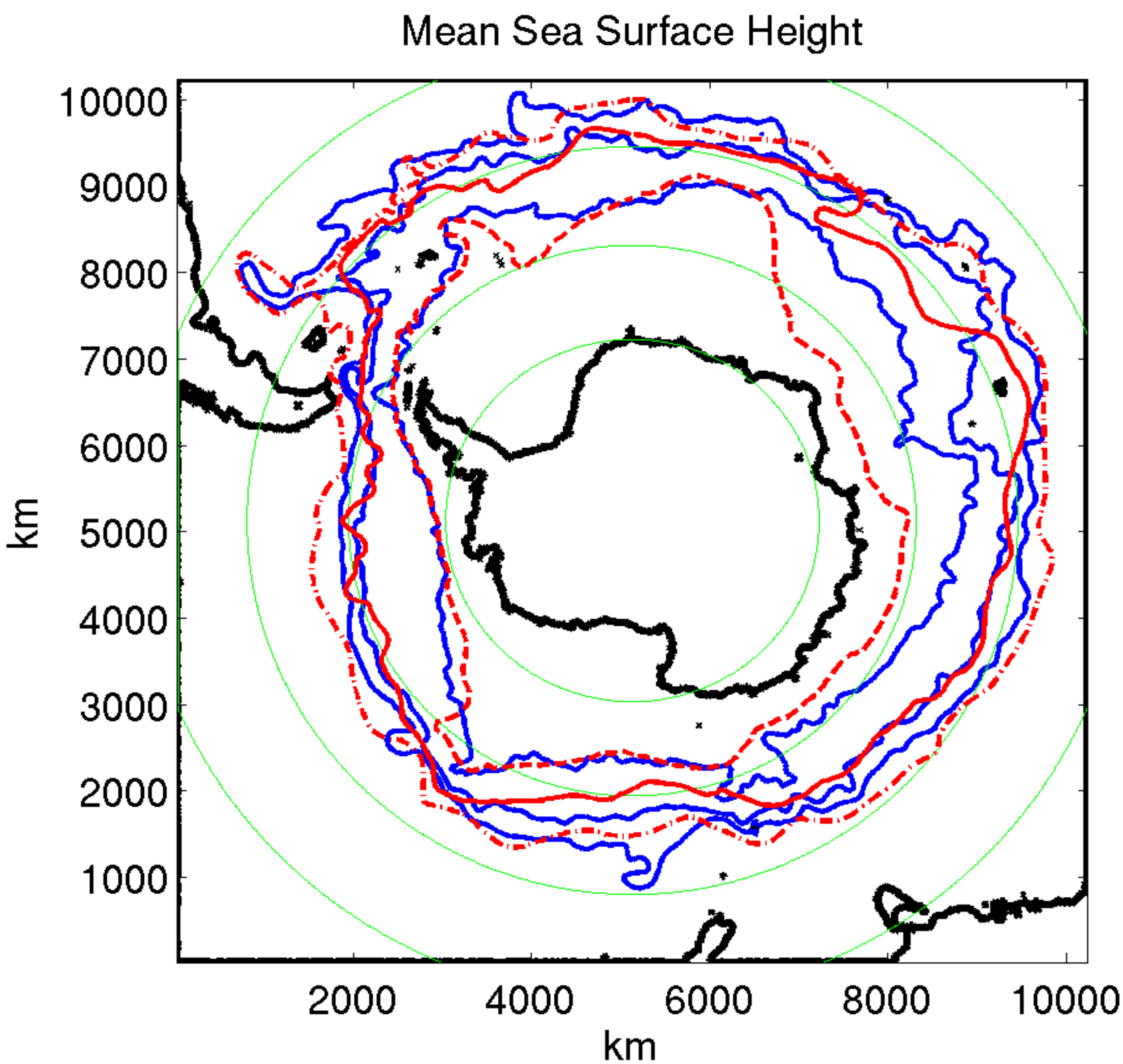

Figure 11. Mean sea surface height (SSH) over the interval 1999 to 2010. Climatological front locations (blue, Orsi et al. 1995) for the Subantarctic, Polar and southern boundary of the ACC are compared to the best fit SSH contour (red) for each front.

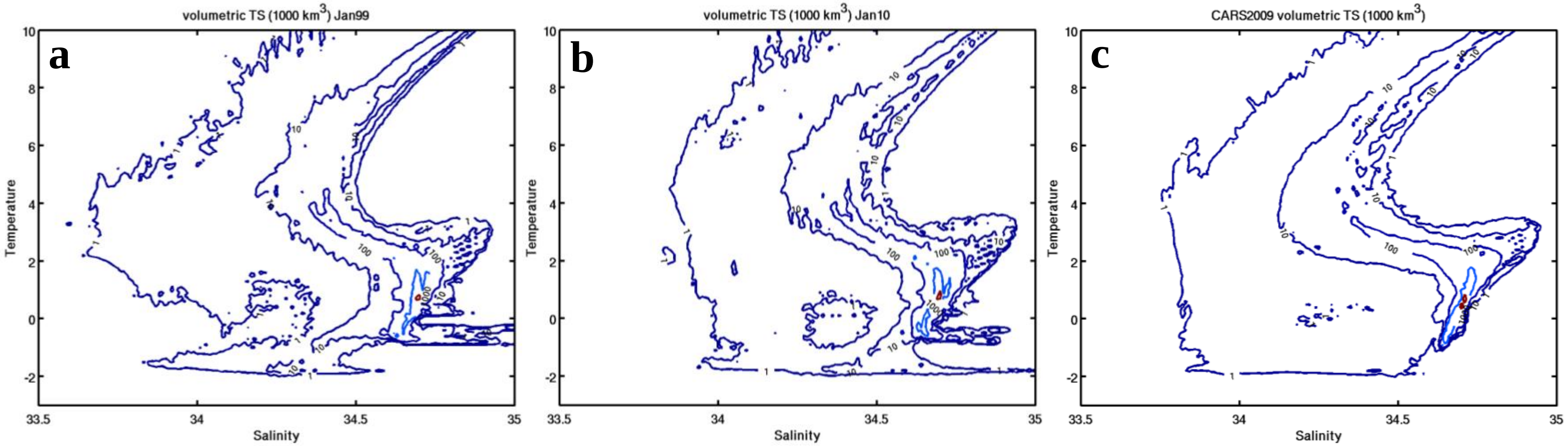

Figure 12. The total volume of water (units of 1000 km^3) for T and S classes with intervals of 0.1°C and 0.01 PSU, respectively, for the ocean. (a) At the beginning of the simulation (January 1999) and (b) at the end of the simulation (January 2010). (c) The CARS climatology for comparison.

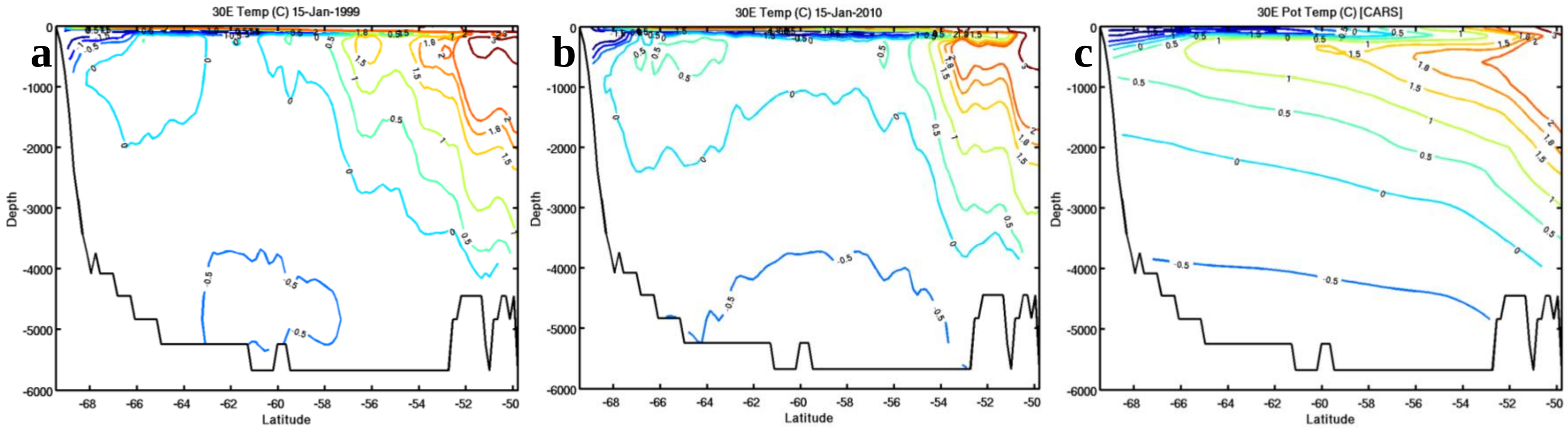

Figure 13. Vertical section for temperature at 30°E extending from the continent to 50°S. (a) January 1999, (b) January 2010, and (c) CARS climatology. The contour interval is 0.5°C from 1 to 1°C. Additional contours are at 2, 5 and 9°C.

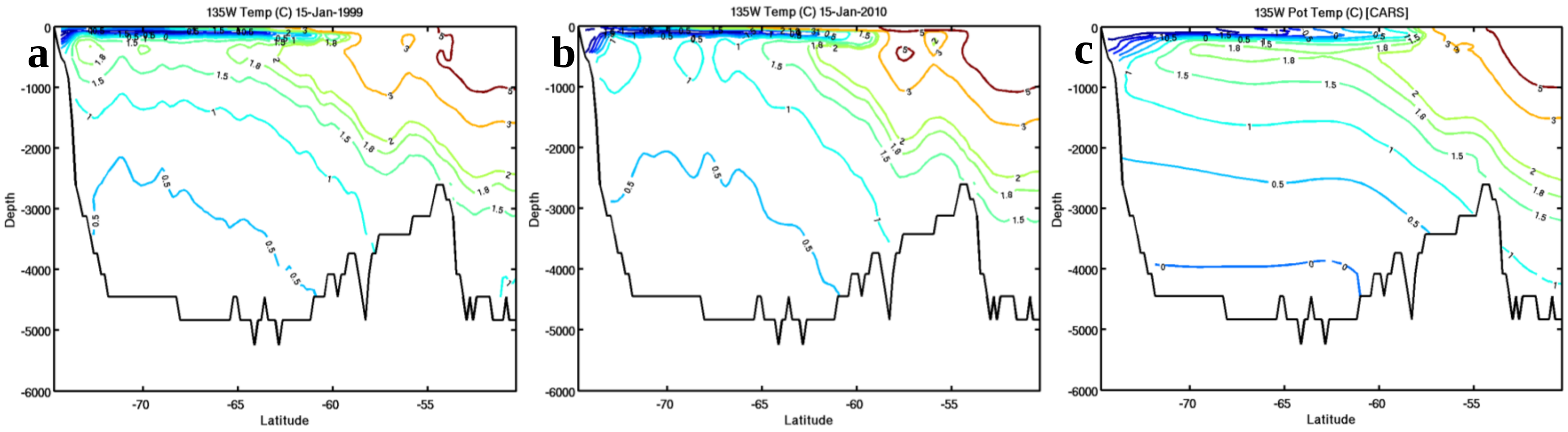

Figure 14. Vertical section for temperature at 135°W extending from the continent to 50°S. (a) January 1999, (b) January 2010, and (c) CARS climatology. The contour interval is 0.5°C from 1 to 1°C. Additional contours are at 2, 5 and 9°C.

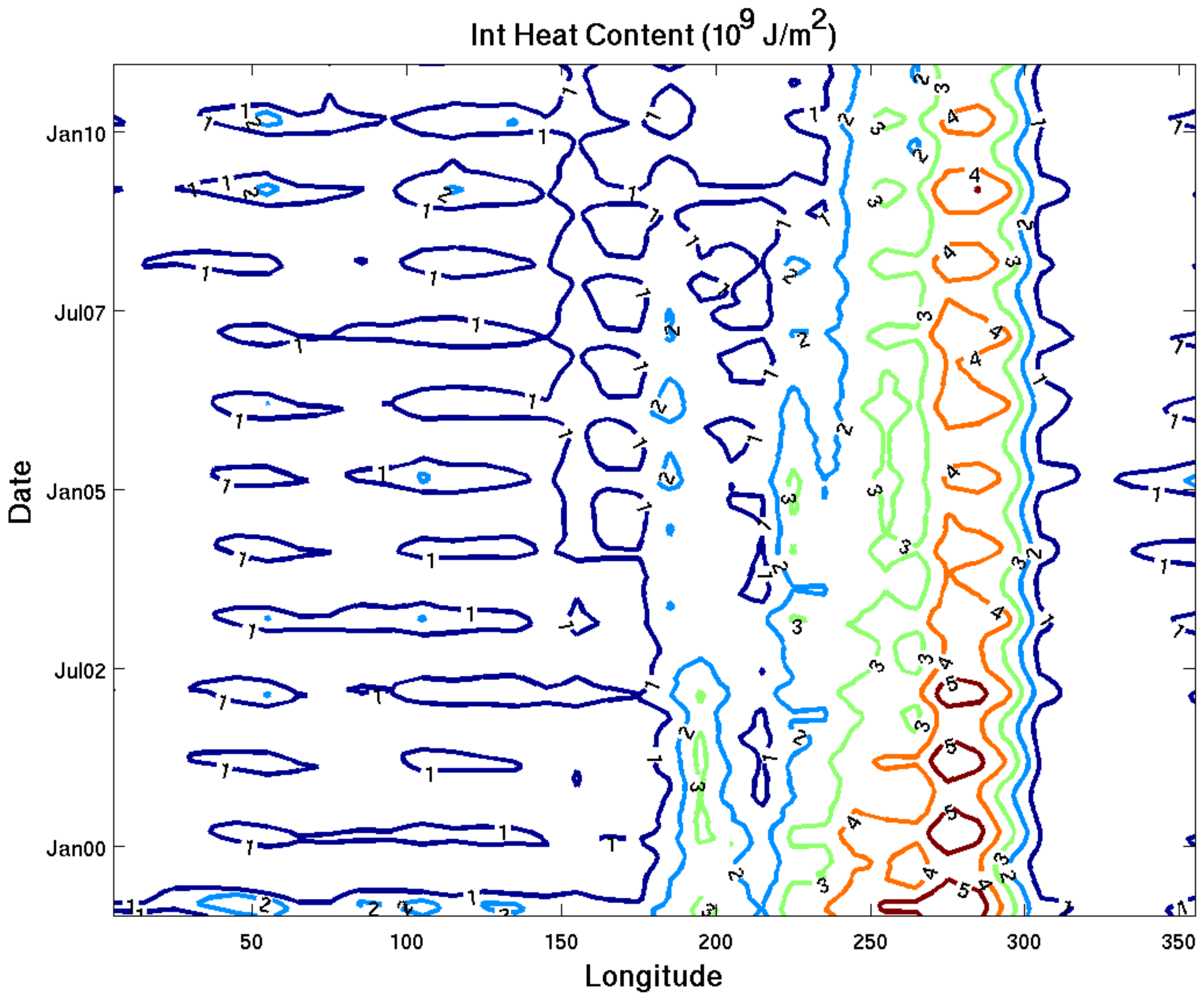

Figure 15. Total heat content for each month for locations south of 60°S with depths less than 635 m over a depth range of 105 m to the bottom. Heat content is integrated over 10° longitude bins.

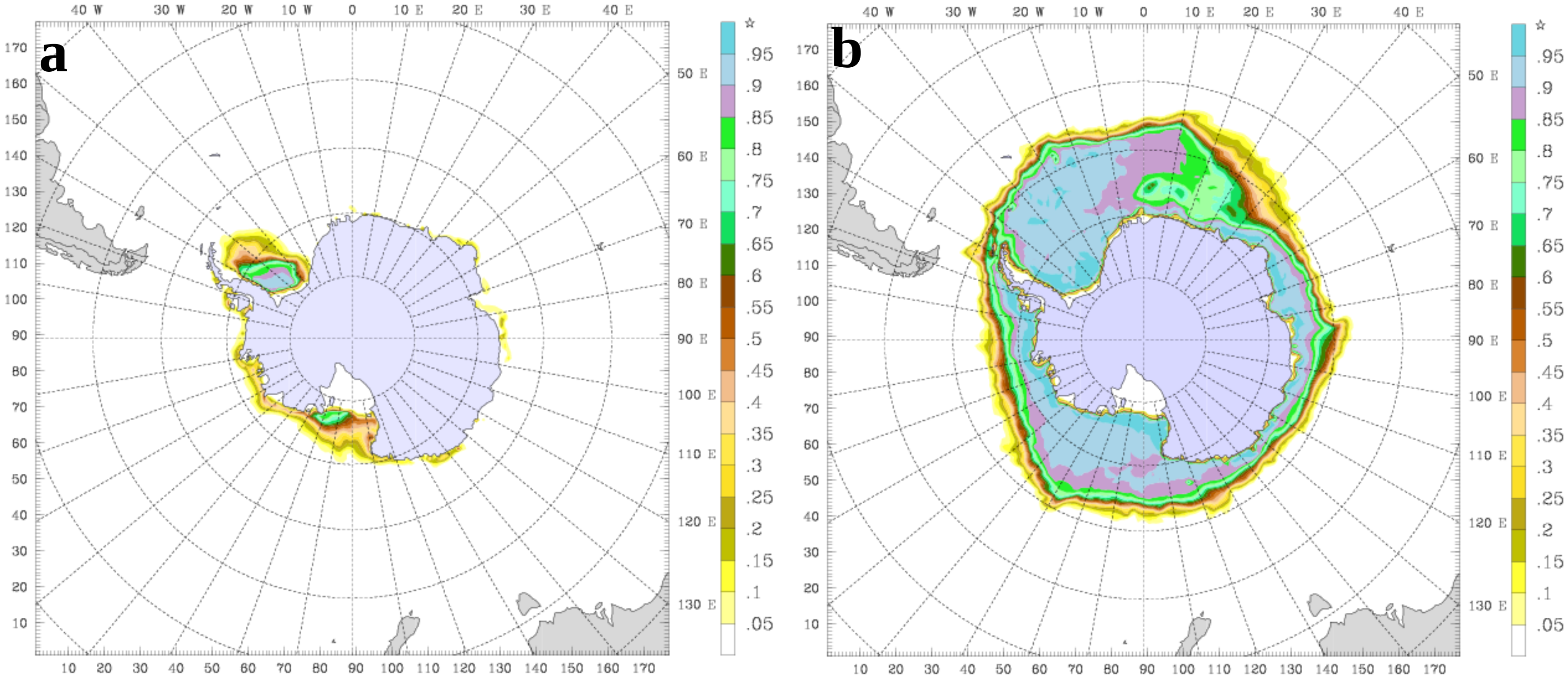

Figure 16. Sea ice concentration (fraction) for (a) March (lowest coverage) and (b) September (highest coverage) averaged for 1999-2010.

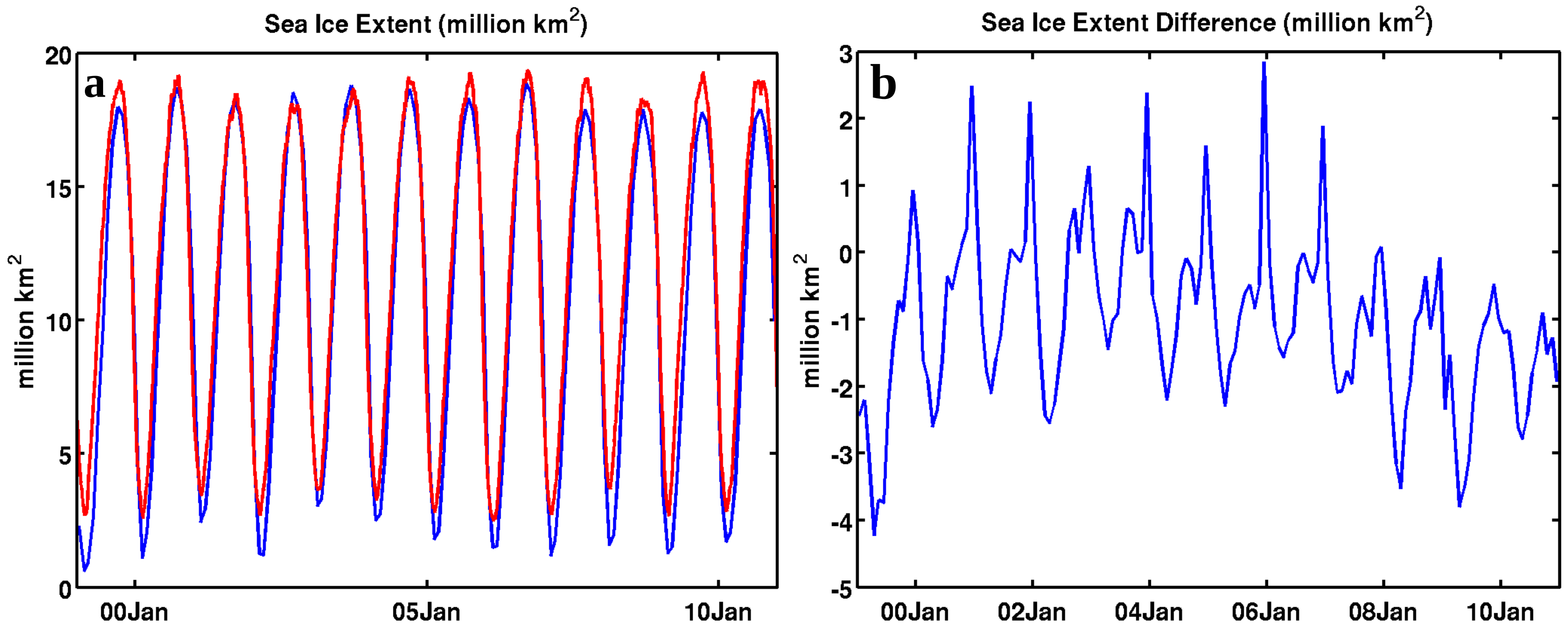

Figure 17. Sea ice extent (total area of ice concentration more than 15%) for each month over the 12 year simulation. (a) Model results are blue; observed (Fetterer et al. 2002) is red. (b) Difference between the model sea ice extent and observations.

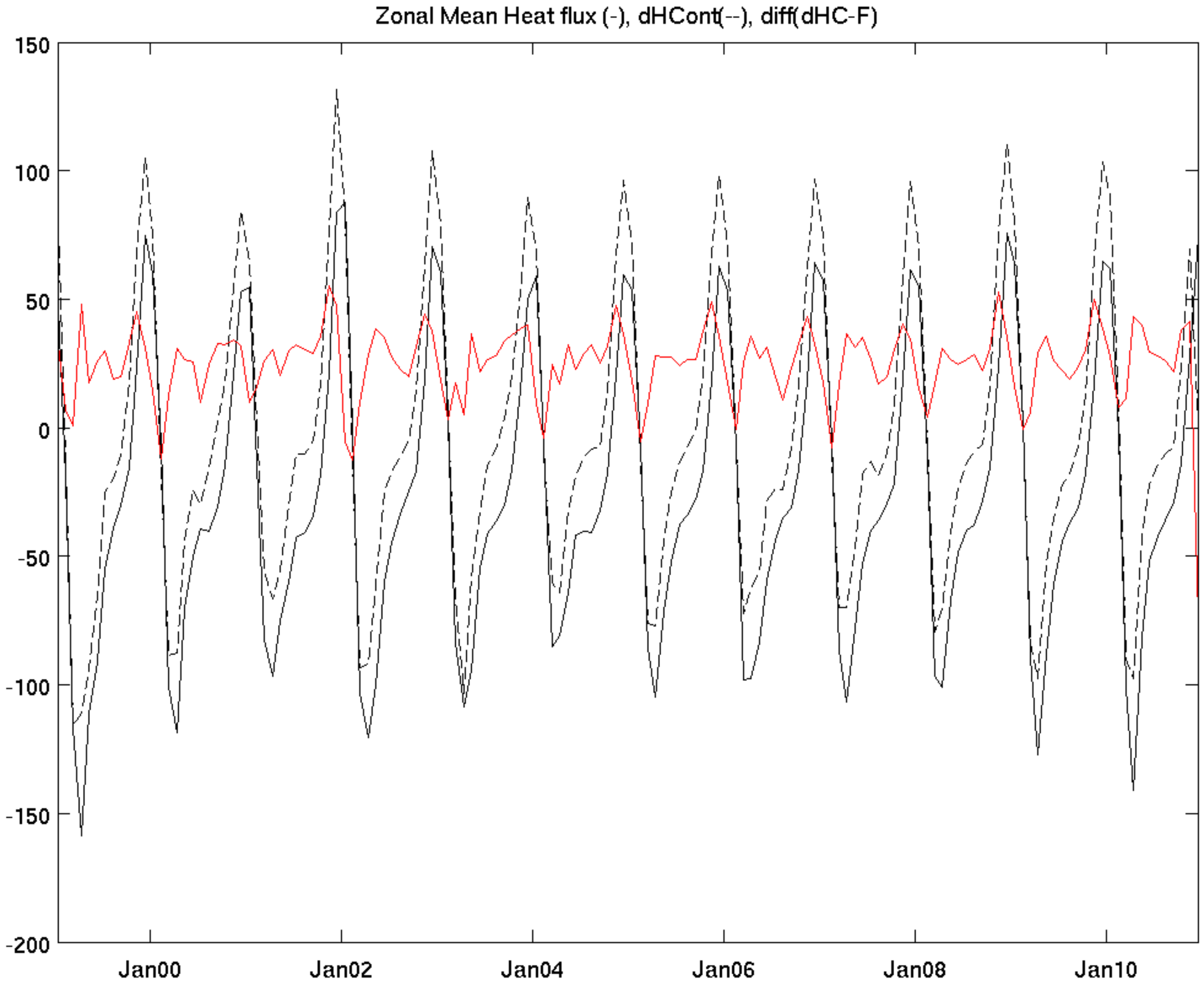

Figure 18. Area-averaged surface heat flux (solid line) and heat content change (dashed line) for shelf areas (defined as model cells south of 60°S with depths less than 630 m). The difference (red line) is an estimate of heat exchange across the shelf break.